

Earthquake Response of a Three-span bridge, with mid-span supported by pins, to Near-field Pulse and Permanent-displacement Step

by

Reza S. Jalali¹, Masoumeh Bahari Jokandan², and Mihailo D. Trifunac³

^{1,2}*Dept. of Civil Eng., Faculty of Eng., University of Guilan, P.O. Box 3756, Rasht, Iran*

³*Dept. of Civil Eng., University of Southern California, Los Angeles, CA, 90089, USA*

ABSTRACT

Wave passage and differential motions of long structures can lead to excessive demands in the near field of strong earthquakes. For long and stiff structures these demands are dominated by pseudo-static deformations resulting from differential ground motions. In our previous work we confirmed that replacing continuous bridge girder with multiple short segments, interconnected by structural joints, reduces the pseudo-static forces in the piers. In this paper, these reductions are further examined for a three-span bridge with mid-span supported by pins. It is shown that the placement of pins in the mid-span, rather than over the piers, results in only minor differences in the forces and drifts of the bridge. The shear forces in the joint keys, as well as the drifts of piers, for out-of-plane response are again reduced in the high frequency band in the bridge that is made flexible by placement of joints in the middle span.

Key words: Out-of-plane response of a three-span bridge, spatial seismic effects, ground rotations, structural torsion, reduction of shear forces in joint keys, reduction of pseudo-static actions.

INTRODUCTION

For large and long structures, the effects of differential earthquake ground motions become significant and should be considered in the design (Bogdanoff et al. 1965; Okubo et al. 1983; Zembaty and Krenk 1993, 1994). Contributions to the response caused by differential ground motion have been studied for beams (Harichandran and Wang 1988, 1990; Zerva 1991), bridges (Kashefi and Trifunac 1986; Perotti 1990; Hyun et al. 1992), simple models of three-dimensional structures (Hao 1991), long buildings (Todorovska and Lee 1989; Todorovska and Trifunac 1989, 1990a, 1990b), and dams (Kojić and Trifunac 1988, 1991a, 1991b).

Extensions and generalizations of the classical response-spectrum method, which are based on the Taylor series approximations of long-wave ground motions, cease to be valid for short-wave excitations. Such extensions have been described in the studies involving differential strong motion (Jalali and Trifunac 2009, 2011; Trifunac and

Todorovska 1997a; Trifunac and Gičev 2006) and the strength-reduction factors (Jalali and Trifunac 2007, 2008; Jalali et al. 2007). Hao (1998) studied the required seating length to avoid unseating and pounding of adjacent bridge decks. Zanardo and Hao (2002) confirmed the significance of the spatially non-uniform ground motions, and Chouw and Hao (2003, 2004, 2005) showed that neglecting the soil-structure interaction (SSI) effect and ground-motion spatial variations will result in inaccurate prediction of pounding responses of bridge girders.

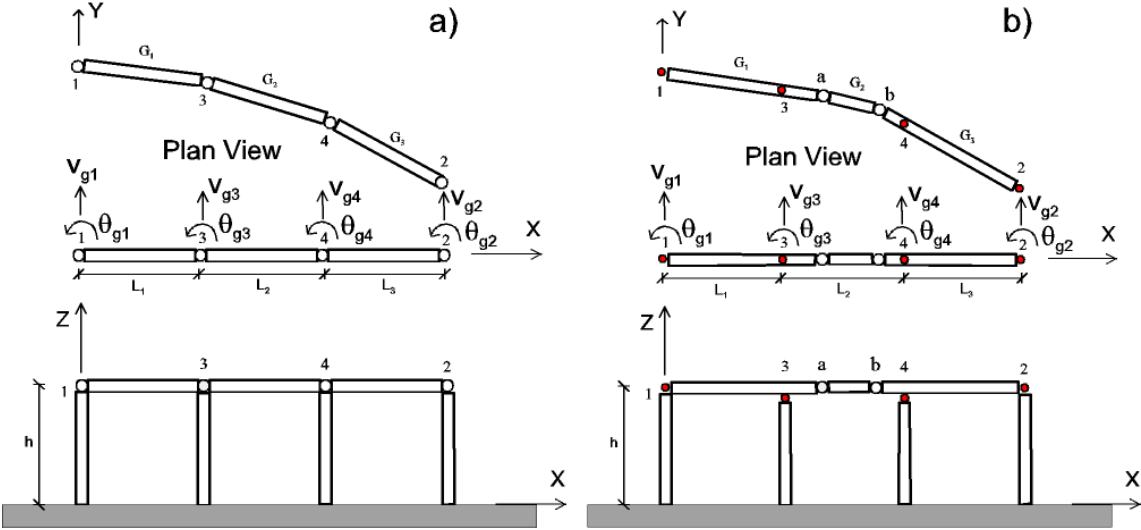


Fig. 1. Plan view (top) and side view (bottom) of the schematic representation of a “bridge” with pins over the columns (from Jalali et al. 2012) (left) and with pins in the central span (right) as studied in this paper

The purpose of this paper is to extend the results of Jalali et al. (2012), who analyzed the seismic response of a simple, symmetric model of a three-span, simply supported bridge (Figure 1a) to fault-parallel and fault-normal displacements near faults. In this paper we study the same bridge, but move the pins of the central span away from the piers, as shown in Figure 1b. To emphasize only the consequences of differential, but propagating and transient fault-normal pulses and fault-parallel displacements, it will be assumed again that the soil-structure interaction can be neglected. Impulsive ground motion near an earthquake fault, and in particular the amplitude and period of the velocity pulses there, can have a significant effect on the performance of structures (Hall et al. 1995; Mylonakis and Reinhorn 2001; Dicleli 2008; Fenves and Ellery 1998; Jonsson et al. 2010; Trifunac and Todorovska 1994; Goel and Chopra 2008). These large pulses in acceleration, velocity and displacement time histories can also propagate to considerable distances from the fault and maintain their amplitudes and polarity over distances as large as tens of km (Todorovska and Trifunac 1997).

This study aims to illustrate qualitatively the dynamic consequences of wave-passage effects on long, bridge-like structures for idealized, near-fault, strong-motion pulses, to show the advantages of the flexible long structure, which can follow the deformations imposed by the propagating waves, and to show that the placement of the joints supporting the central span does not alter the overall trends in the response. A sensitivity analysis of the dependence of the response on many other governing variables and of the range of their possible values is beyond the scope of this paper. In this paper we consider only the wave passage effects. We do not consider coherency loss, which is poorly understood and difficult to model in the near field.

DYNAMIC MODEL

The model we consider is a symmetric three-span bridge with middle hinges at a and b from the central columns (Figure 1b) consisting of three rigid decks with masses m_1, m_2, m_3 , polar mass moments of inertia J_1, J_2, J_3 , and lengths L_1, L_2, L_3 , supported by four axially-rigid mass-less piers connected at the top to the deck and at the bottom to the ground by circular rotational and torsional springs. The rotational and torsional springs represent the bending and torsional stiffness of the piers. It is assumed that there is no soil structure interaction so that the points on ground surface where the piers are supported move as in the free field of strong motion. At the middle hinges the rigid decks are interconnected by rigid shear keys to prevent out-of-plane relative displacement and unseating. The mass-less piers are connected to ground and to the rigid deck by linear circular rotational and torsional dashpots providing the prescribed fraction of critical damping. Rotation of the piers is assumed to be small enough so that the interaction between in-plane and out-of-plane motions of the rigid decks may be neglected. The bridge is acted upon by the acceleration of gravity, g , and is excited by differential out-of-plane and torsional ground motions. This model and its governing equations are described in Appendix A.

NEAR-FAULT GROUND MOTION

To describe the ground motion near faults we consider d_F (fault-normal pulse) and d_N (fault-parallel permanent displacement), and select their amplitudes and duration to be consistent with what is known about the nature of these motions near-faults. Figure B1 in Appendix B shows schematically a fault and these two characteristic motions, d_N and d_F , which describe monotonic growth of the displacement toward the permanent static offset, and a pulse, here assumed to be perpendicular to the fault and associated with failure of a nearby asperity or passage of dislocation under or past the observation point. Further discussion and motivation for selecting these simple strong-motion displacement functions can be found in author's previous work (Jalali and Trifunac 2007, 2008, 2009).

The motions d_N and d_F have large initial velocity. It is proportional to the stress drop on the fault, and even in the presence of nonlinear site response it can be in the range of hundreds of cm/s (Trifunac 1998, 2009)

STRUCTURAL RESPONSE

As in Jalali et al. (2012), it is assumed that $L_1=L_2=L_3=L=30\text{ m}$, and for different phase velocities different time delays τ will be selected ($\tau = .03, .05, .1, .2, .3\text{ s}$). The height of the bridge is $h=6\text{ m}$, and the torsional stiffness of piers is neglected ($K_{TC} = 0$). The contribution of all modes of the bridge is included in all analyses and the damping ratio of the first mode is supposed to be $\zeta_1 = 0.02$. The period of the first mode of the bridge is assumed to vary between $T_1=0.1$ and 1.5 sec and all the results are shown versus T_1 . In nonlinear analyses, the material behavior of piers in bending is assumed to be elasto-plastic and the yielding limit of rotational springs of piers is supposed to be $\phi_y = 0.005$ and 0.01 .

In this paper only the action of out-of-plane (along the Y-axis, Figure 1) component of near-fault ground motion will be considered at the base of the piers (v_{g_i}) for earthquake magnitudes $M = 4-7$, but the effects of foundation-soil interaction will be neglected. It is assumed that the bridge is near a fault and that the longitudinal axis of the bridge (X-axis) coincides with the radial direction (r-axis) of the propagation of waves from the earthquake source so that the absolute displacements of the bases of piers because of the wave passage are different. It is further assumed that the ground motion can be described approximately by linear-wave motion. Thus, the nonlinear soil strains and cracks in the soil, which accompany violent, strong ground motion in the near field will not be considered (Trifunac and Todorovska 1996; 1997a,b,c; Trifunac et al. 1996). By considering the wave propagation from left to right in Figure 1b, it is assumed that the excitations at all four piers have the same amplitude but differ in terms of phase. The phase difference (or time delay τ) between the four ground motions depends on the distance between piers and the horizontal phase velocity of the incident waves. As can be seen in Figure 1b, the system is excited by differential out-of-plane ground motions, $v_{g_i}, i = 1, 4$, at the four bases, so that

$$\begin{aligned} v_{g_2}(t) &= v_{g_1}(t - \tau) \\ v_{g_3}(t) &= v_{g_1}(t - \tau/3) \\ v_{g_4}(t) &= v_{g_1}(t - 2\tau/3) \\ \tau &= (3L)/C_x \end{aligned} \quad (1)$$

where C_x is the horizontal phase velocity of incident waves. The functional form of $v_{g_i}(t)$ is defined by Equations (B1) and (B2) (see Appendix B) for the fault-normal pulse and fault-parallel displacements, respectively. For body waves, C_x will depend on the shear-wave velocity in the half space (β) and the incident angle (γ). For surface waves, C_x will depend on the dispersion characteristics of the medium (note that $C_x(\omega)$ will be different for each of the surface-wave modes; Todorovska et al. 2013). For plane

waves, the value of C_x varies between β and infinity: ($\beta < C_x < \infty$), and in this paper, it will be assumed to vary between 300 m/s and infinity ($300 < C_x < \infty$).

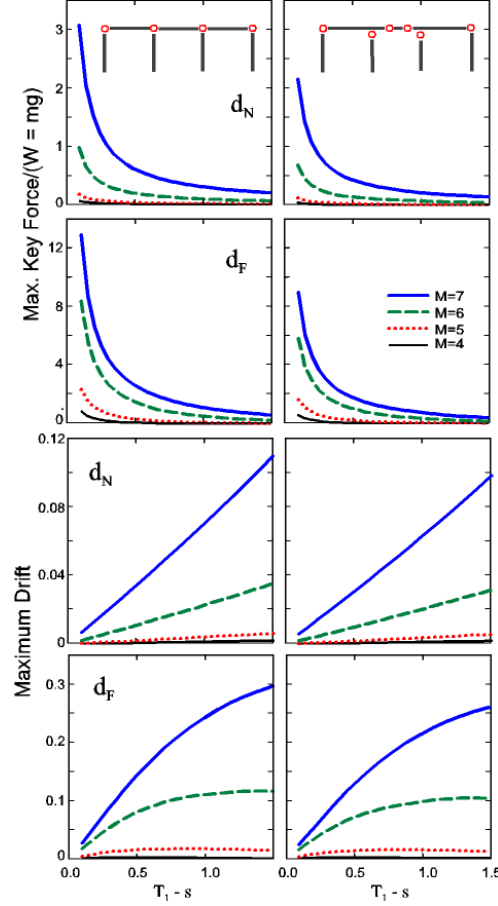


Fig. 2. Maximum linear-shear-key forces (top two levels), and drifts in the piers (bottom two levels) vs. the fundamental period (T_1), for fault-parallel displacement d_N and fault-normal pulse d_F , for magnitudes $M = 4$ to 7 , for $\tau = 0$ and $K_{TC} = 0$, and for the bridge models with pins over the columns (left) and in the central span (right)

For each specific design of a bridge, there will exist some torsional resistance between deck ends and piers. In Jalali et al. (2012), the torsional resistance between the middle piers and the deck ends at the two sides was modeled by a torsional spring with stiffness $0.5 K_{TC}$, and the torsional resistance between the end piers and the deck ends was modeled by torsional springs with stiffness K_{TC} , where K_{TC} is the torsional stiffness of the piers (Figure A1c). The ratio of torsional to bending stiffness for each pier (K_{TC} / K_ϕ) depends on the number of columns at each pier, the width of the bridge and the piers, the distance between the columns of each pier, the cross section and the height of the columns of each pier, and their material properties (Figure A1d). The ratio of K_{TC} / K_ϕ is expected to vary between 0.1 and 2.0 (Jalali et al. 2012).

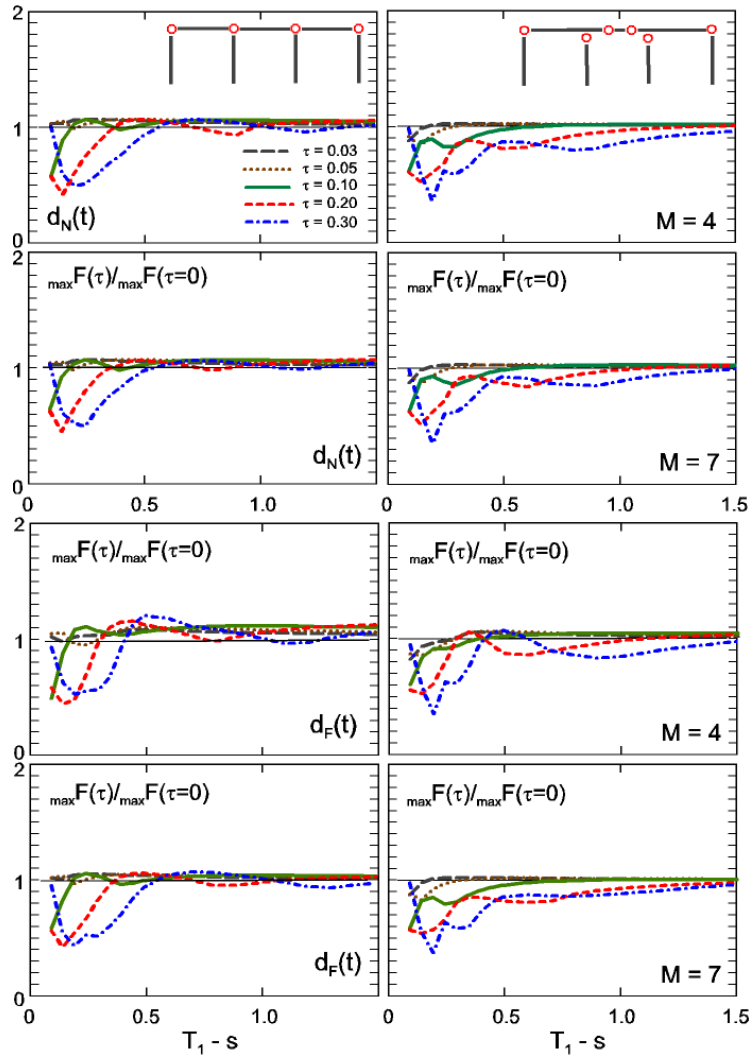


Fig. 3. Wave-passage effects on magnification factor of maximum linear-shear-key forces vs. system fundamental period (T_1), time lag τ in seconds, for $K_{TC} = 0$, for excitation by fault-parallel displacement d_N (top four segments), and for fault-normal excitation by d_F (bottom four segments), for magnitudes $M = 4$ and 7 , and for the bridge models with pins over the columns (left) and in the central span (right)

RESULTS

Based on the above formulation (Equation A8) we analyzed the response of a three-span bridge with middle shear keys and different main periods excited by fault-parallel and fault-normal displacements for different earthquake magnitudes and time lags of wave arrival to the base of the columns. The linear response of the bridge is shown in figures 2 through 4 and the nonlinear response of the system is presented in figures 5 through 8.

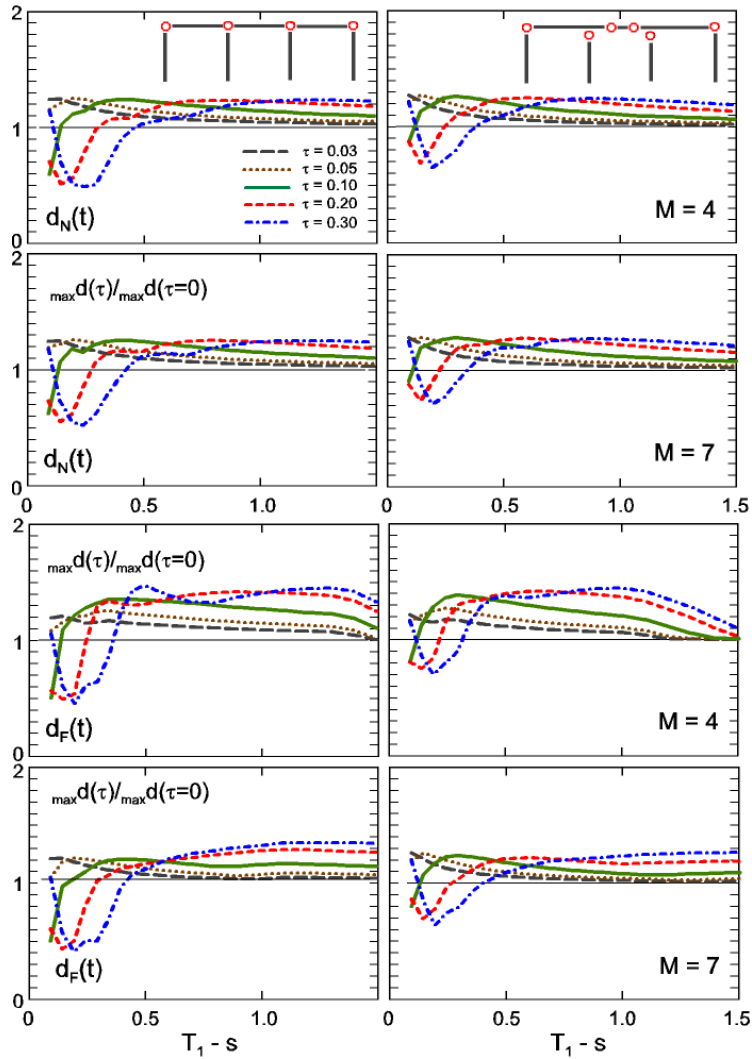


Fig. 4. Magnification factor of maximum linear drift in the piers of the bridge, vs. system fundamental period (T_1) and time lag τ in seconds, with $K_{TC} = 0$, for fault-parallel displacement d_N (top four segments), fault-normal pulse d_F (bottom four segments), for earthquake magnitudes $M = 4$ and 7 , and for the bridge models with pins over the columns (left) and in the central span (right)

As it is seen from Figure 2 the same trends in the response are present as in the paper by Jalali et al. (2012) (Figure 1a). It is seen that the maximum shear key forces and drifts in the piers induced by fault-normal pulse are more than those induced by fault-parallel displacement. By increasing of the main period of the bridge the maximum shear key forces decreases while the maximum drift in pier increases. For excitation by fault-parallel displacement the maximum shear key forces and drifts in piers may increase up to $2g$ and 10 percent for stiff ($T_1=0.1$ sec) and soft ($T_1=1.5$ sec) bridges, respectively. Meanwhile for excitation by fault-normal pulse the corresponding values may increase up to $9g$ and 25 percent, respectively.

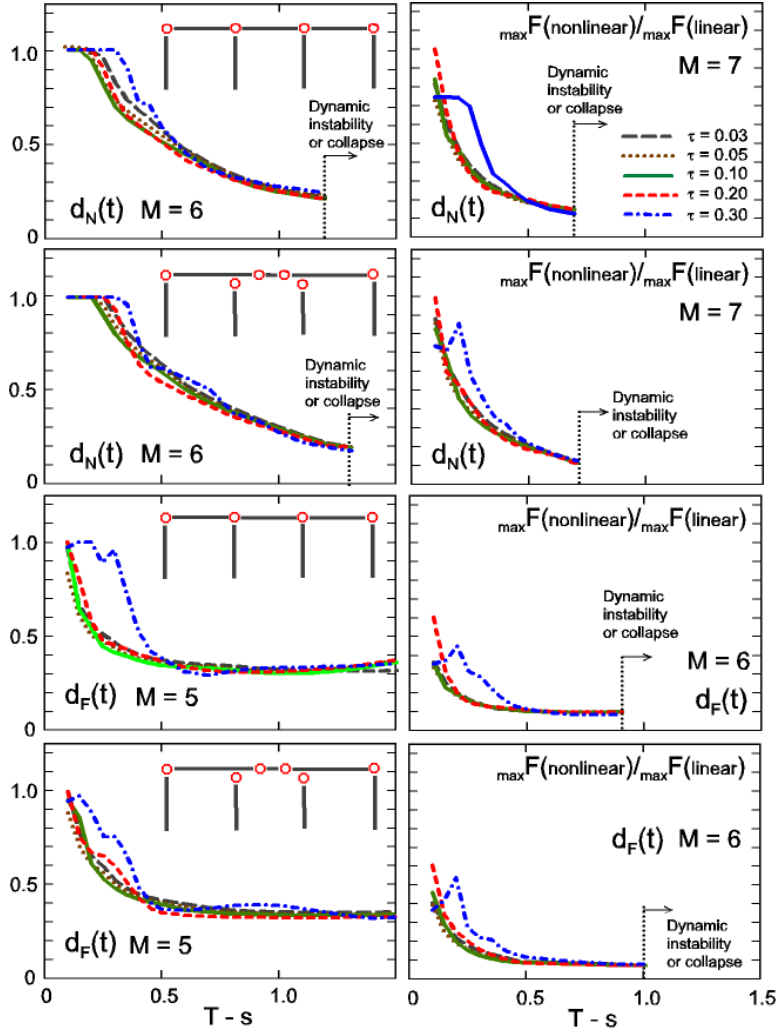


Fig. 5. Ratios of maxima during nonlinear system response to maxima, during the linear system response, of the shear-key forces vs. system fundamental period (T_1) and time lags τ (in seconds) for $K_{TC} = 0$ and $\phi_y = 0.005$, excited by fault-parallel displacement d_N and magnitudes $M = 6$ and 7 (top four segments), and by fault-normal pulse d_F and magnitudes $M = 5$ and 6 (bottom four segments), for the bridge models with pins over the columns (top and third rows) and in the central span (second and bottom rows)

In Figures 3 and 4 we show the effects of wave passage on the maximum shear key forces and drifts in piers of bridge for different earthquake magnitudes. As seen from Figures 3 under near fault ground motions the differential motion effect on maximum shear key forces of bridge is negligible in entire range of considered periods. Meanwhile the wave passage of translational out-of-plane excitation can increase drifts by 25 to 40 percent for all magnitudes and depending to the time delay and due to the combined action of out-of-plane and torsional response this amplification can occur in entire range of considered periods ($0.1 < T_1 < 1.5$).

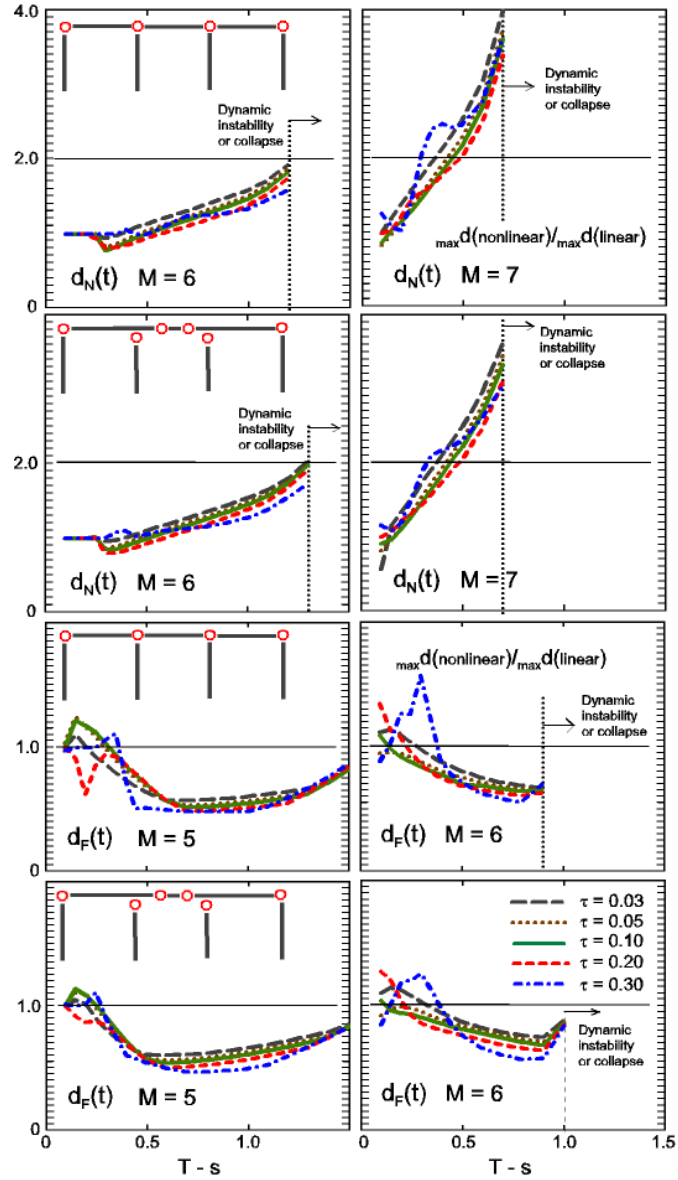


Fig. 6. Ratios of maximum drifts during nonlinear response to the maximum drifts during linear response in the piers of the bridge, vs. system fundamental period (T_1) and time lags τ (in seconds), for $K_{TC} = 0$, and $\phi_y = 0.005$, excited by fault-parallel displacement d_N with magnitudes $M = 6$ and 7 (top four segments), and by fault-normal pulse d_F with magnitudes $M = 5$ and 6 (bottom four segments), for the bridge models with pins over the columns (top and third rows) and in the central span (second and bottom rows)

By assuming material nonlinearity in bending of piers we show the ratio of nonlinear to linear response of the bridge in Figures 5 through 8. Again we find the same trends as for the model in Figure 1a. Depending on the main period of the bridge, earthquake magnitude, and ϕ_y the amplitude of the responses become sensitive to action of the

gravity load. For large magnitudes and small ϕ_y , the destabilizing effect of gravity and of horizontal excitation lead to conditions that are close to collapse ($\phi > \phi_s$). As it is seen from Figures 5 through 8 under near-fault ground motions the nonlinear behavior of piers tends to decrease the maximum shear key forces relative to what occurs in the linear system. For excitation by fault-parallel displacement the nonlinear behavior of piers tends to increase in maximum drift in piers of the bridge. Meanwhile, under fault-normal pulse this trend is not seen and nonlinear behavior of piers tends to a decrease in maximum drift in the range of considered periods.

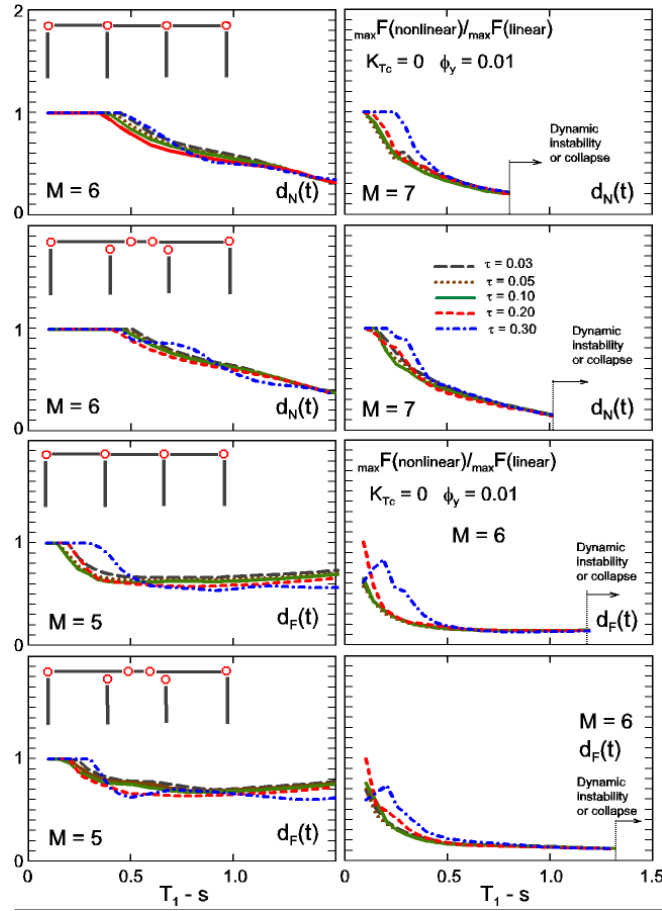


Fig. 7. Ratios of maxima during nonlinear response to the maxima during linear response, of the shear-key forces vs. system fundamental period (T_1) and time lags τ (in seconds), for $K_{TC} = 0$, and $\phi_y = 0.01$, excited by fault-parallel displacements d_N with magnitudes $M = 6$ and 7 (top four segments), and by fault-normal pulses d_F with magnitudes $M = 5$ and 6 (bottom four segments), for the bridge models with pins over the columns (top and third rows) and in the central span (second and bottom rows)

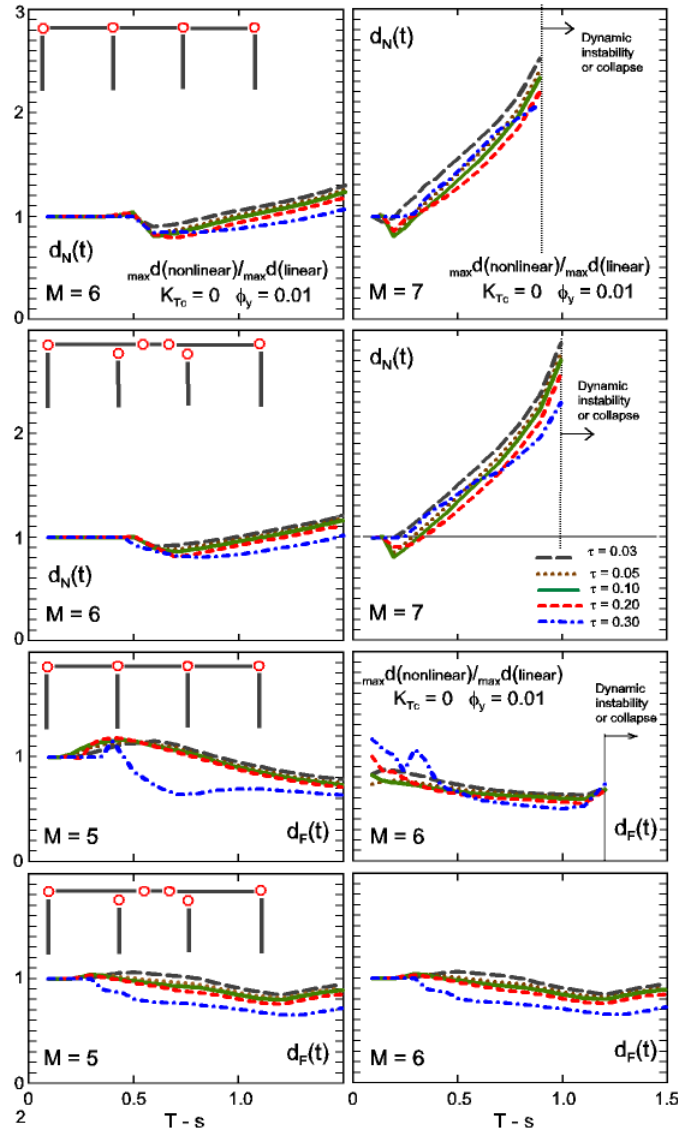


Fig. 8. Ratios of maximum drifts in the piers during nonlinear response to the drifts during linear response, vs. system fundamental period (T_1) and time lags τ (in seconds), for $K_{TC} = 0$, and $\phi_y = 0.01$, excited by fault-parallel displacements d_N with magnitudes $M = 6$ and 7 (top four segments), and by fault-normal pulses d_F with magnitudes $M = 5$ and 6 (bottom four segments), for the bridge models with pins over the columns (top and third rows) and in the central span (second and bottom rows)

DISCUSSION AND CONCLUSIONS

The results of this study show that, with only a few exceptions, the key forces between the bridge piers and bridge decks are reduced for τ greater than zero relative to the synchronous excitation ($\tau = 0$) during linear system response to the propagating excitations by d_N and d_F (fault-parallel displacement and fault-normal pulse,

respectively). The exceptions to this occur only in the end span (span 4-2 in Figures 1a and b) and are associated with out-of-plane whipping as the displacements d_N and d_F leave the ground beneath the bridge and propagate out to the right. The reductions are more significant for long transit times τ , longer than ~ 0.1 s, and mainly occur for “stiff” piers when T_1 is approximately between 0.1 and 0.3 s. This is due to the ability of the deck to deform by following the out-of-plane ground motion by relative rotation of the decks about the vertical axes through the piers at pins 3 and 4 (Figures 1a and b). As would be expected, these reductions become smaller, and magnification factors become larger than 1, for very small T_1 , and as the torsional stiffness between adjacent decks increases (Jalali et al. 2012). Also, the results of the simply supported model show that the wave-passage effects lead to increases of about 25% to 40% in the drift of the piers.

In the absence of the pins, a long and continuous deck would have resulted in larger shear forces and bending moments in the piers during out-of-plane excitation with nonzero transit times (Jalali and Trifunac 2011; Jalali et al. 2012; Trifunac and Gičev 2006). Long, continuous decks have large inertia, and through their large longitudinal rigidity they force all relative displacements between the deck and the ground to be taken by the piers. The rigid girders thus place larger demands on the piers.

The forces in the shear keys for the bridge models in Figures 1a and b are further reduced significantly by the nonlinear response of the piers (Figures 5 to 8), as long as the drifts in the piers are smaller than the angles, which lead to collapse caused by the gravity loads, dynamic instability, or both. Once again, it has been shown that for bridges and long structures on multiple supports the internal forces can be significantly reduced by selecting structural systems that can deform and conform to the motions imposed by the ground waves.

REFERENCES

- Bogdanoff, JL, Goldberg, JE, and Schiff, AJ 1965. “The effect of ground transmission time on the response of long structures”, *Bulletin of the Seismological Society of America*, Vol. 55, No. 3, pp. 627–640.
- Chouw, N, and Hao, H 2003. “Effect of simultaneous spatial near-source ground excitation and soil on the pounding response of bridge girders”, *Journal of Applied Mechanics JSCE* Vol. 6, pp. 779–788.
- Chouw, N and Hao, H 2004. “Investigation of soil-structure interaction and near-source ground motion spatial variation effect on pounding of bridge girders” *Proceedings of the 11th international conference on soil dynamics and earthquake engineering and the third international conference on earthquake geotechnical engineering*, University of California, Berkeley, CA, pp. 726–733.

Chouw, N and Hao, H 2005. "Study of SSI and non-uniform ground motion effect on pounding between bridge girders", *Soil Dynamics and Earthquake Engineering*, Vol. 25, pp. 717–728.

Dicleli, M 2008. "Performance of seismic-isolated bridges with and without elastic-gap devices in near-fault zones", *Earthquake Engineering and Structural Dynamics*, Vol. 37 pp. 935–954.

Fenves, GL and Ellery, M 1998, "Behavior and Failure Analysis of a Multiple-Frame Highway Bridge in the 1994 Northridge Earthquake", Report No. PEER 98/08, Pacific Earthquake Engineering Research Center, College of Engineering, University of California, Berkeley, CA.

Goel, RK and Chopra, AK 2008. "Role of shear keys in seismic behavior of bridges crossing fault-rupture zones", *Journal of Bridge Engineering*, Vol. 13, No. 4, pp. 398–408.

Hall, JF, Heaton, TH, Halling, MW and Wald, DJ 1995. "Near source ground motion and its effects on flexible buildings", *Earthquake Spectra*, Vol. 11, pp. 569–606.

Hao, H 1991, "Response of multiply supported rigid plate to spatially correlated seismic excitation", *Earthquake Engineering and Structural Dynamics*, Vol. 20, No. 9, pp. 821–838.

Hao, H 1998. "A parametric study of the required seating length for bridge decks during earthquakes", *Earthquake Engineering and Structural Dynamics*, Vol. 27, pp. 91–103.

Harichandran, RS and Wang, W 1998. "Response of simple beam to spatially varying earthquake excitation", *Journal of Engineering Mechanics Division, ASCE*, Vol. 114, No. 9, pp. 1526–1541.

Harichandran, RS and Wang, W 1990. "Response of intermediate two-span beam to spatially varying seismic excitation", *Earthquake Engineering and Structural Dynamics*, Vol. 19, No. 2, pp. 173–187.

Haskell, NA 1969. "Elastic displacements in the near field of a propagating fault", *Bulletin of Seismological Society of America*, Vol. 59, No. 2, pp. 956–980.

Hyun, CH, Yun, CB and Lee, DG 1992. "Nonstationary response analysis of suspension bridges for multiple support excitations", *Probabilistic Engineering Mechanics*, Vol. 7, No. 1, pp. 27–35.

Jalali, RS and Trifunac, MD 2007. "Strength-reduction factors for structures subjected to differential near-source ground motion", *Indian Society of Earthquake Technology Journal*, Vol. 44, No. 1, pp. 285–304.

Jalali, RS and Trifunac, MD 2008. “A note on strength reduction factors for design of structures near earthquake faults”, *Soil Dynamics and Earthquake Engineering*, Vol. 28, No. 3, pp. 212–222.

Jalali, RS and Trifunac, MD. 2009. “Response spectra for near-source, differential and rotational strong ground motion”, *Bulletin of Seismological Society of America*, Vol. 99, No. 2B, pp. 1404–1415.

Jalali, RS and Trifunac, MD 2011. “A note on the wave-passage effects in out-of-plane response of long structures to strong earthquake pulses”, *Soil Dynamics and Earthquake Engineering*, Vol. 31, No. 12, pp. 640–647.

Jalali, RS, Trifunac, MD, Ghodrati Amiri, G and Zahedi, M 2007. “Wave-passage effects on strength-reduction factors for design of structures near earthquake faults”, *Soil Dynamics and Earthquake Engineering*, Vol. 27, No. 8, pp. 703–711.

Jalali, RS, Jokandan, MB and Trifunac, MD 2012. “Earthquake Response of a Three-span Simply-supported Bridge to Near Field Pulse and Permanent Displacement Step”, *Soil Dynamics and Earthquake Engineering*, Vol. 44. pp. 380-397.

Jonsson, MH, Bessason, B and Haflidason, E 2010. “Earthquake response of a base-isolated bridge subjected to strong near-fault ground motion”, *Soil Dynamics and Earthquake Engineering*, Vol. 30, pp. 447–455.

Kashefi, I and Trifunac, MD 1986. “Investigation of Earthquake Response of Simple Bridge Structures”, Department of Civil Engineering, Report No. CE 86-02, University of Southern California, Los Angeles, CA.

Kojić, S and Trifunac, MD 1988. “Earthquake Response of Arch Dams to Non-uniform Canyon Motion”, Department of Civil Engineering, Report No. CE 88-03, University of Southern California, Los Angeles, CA.

Kojić, S and Trifunac, MD 1991a. “ Earthquake stresses in arch dams: I—Theory and anti-plane excitation”, *Journal of Engineering Mechanics Division ASCE*, Vol. 117, No. 3, pp. 532–552.

Kojić, S and Trifunac, MD 1991b. “ Earthquake stresses in arch dams: II—Excitation by SV, P and Rayleigh waves”, *Journal of Engineering Mechanics Division ASCE*, Vol. 117, No. 3, pp. 553–574.

Luco, JE, Trifunac, MD and Wong, HL 1987. “On the apparent change in dynamic behavior of a 9-story reinforced-concrete building”, *Bulletin of Seismological Society of America*, Vol. 77, No. 6, pp. 1961–1983.

Mavroeidis, GP, Dong, and Papageorgiou, AS 2004. “Near-fault ground motions, and the response of elastic and inelastic single-degree-of-freedom (SDOF) systems”, *Earthquake Engineering and Structural Dynamics*, Vol. 33, No.9, pp. 1023–1049.

Mylonakis, G and Reinhorn, AM 2001. "Yielding oscillator under triangular ground acceleration pulse", *Journal of Earthquake Engineering*, Vol. 5, pp. 225–251.

Okubo, T, Arakawa, T and Kawashima, T 1983. "Preliminary Analysis of Finite Ground Strains Induced During Earthquake and Effect of Spatial Ground Motions on Structural Response", *International Symposium on Lifeline Earthquake Engineering*, 4th U.S. National Conference on Pressure Vessels and Piping Technology, ASME, Portland, OR.

Perotti, P 1990. "Structural response to non-stationary multiple support random excitation", *Earthquake Engineering and Structural Dynamics*, Vol. 19, No. 4 pp. 513–527.

Todorovska, MI and Lee, VW 1989. "Seismic waves in buildings with shear walls or central core", *Journal of Engineering Mechanics Division ASCE*, Vol. 115, No.12 pp. 2669–2686.

Todorovska, MI and Trifunac, MD 1989. "Anti-plane earthquake waves in long structures", *Journal of Engineering Mechanics Division ASCE*, Vol. 115, No.12 pp. 2687–2708.

Todorovska, MI and Trifunac, MD 1990a. "A note on the propagation of earthquake waves in buildings with soft first floor", *Journal of Engineering Mechanics Division ASCE*, Vol. 116, No. 4, pp. 892–900.

Todorovska, MI and Trifunac, MD 1990b. "A note on excitation of long structures by ground waves", *Journal of Engineering Mechanics Division ASCE*, Vol. 116, No. 4, pp. 952–964.

Todorovska, MI and Trifunac, MD 1997. "Amplitudes, Polarity and Time of Peaks of Strong Ground Motion During the 1994 Northridge, California Earthquake", *Soil Dynamics and Earthquake Engineering*, Vol.16, No. 4, pp. 235-258.

Todorovska, MI, Trifunac, MD , Lee VW and Orbović, N 2013. "Synthetic Earthquake Ground Motions on an Array, *Soil Dynamics and Earthquake Engineering* (in press).

Trifunac, MD 1974. "A three-dimensional dislocation model for the San Fernando, California, earthquake of February 9, 1971", *Bulletin of Seismological Society of America*, Vol. 64, No.1, pp. 149–172.

Trifunac, MD 1993a. "Long period Fourier amplitude spectra of strong motion acceleration", *Soil Dynamics and Earthquake Engineering*", Vol.12, No. 6, pp. 363–382.

Trifunac, MD 1993b. "Broad band extension of Fourier amplitude spectra of strong motion acceleration", *Department of Civil Engineering Report CE 93-01*, University of Southern California, Los Angeles, CA.

Trifunac, MD 1997. “Relative earthquake motion of building foundations”, *Journal of Structural Engineering*, ASCE, Vol. 123, No. 4 pp. 414–422.

Trifunac, MD 1998. “Stresses and intermediate frequencies of strong motion acceleration”, *Geofizika*, Vol. 14, pp. 1–27.

Trifunac, MD 2009. “The role of strong motion rotations in the response of structures near earthquake faults”, *Soil Dynamics and Earthquake Engineering*, Vol. 29, No. 2 pp. 382–393.

Trifunac, MD and Gičev, V 2006. “Response spectra for differential motion of columns, Paper II: Out-of-plane response”, *Soil Dynamics and Earthquake Engineering*, Vol. 26, No. 12, pp. 1149–1160.

Trifunac, MD and Todorovska, MI 1994. “Broad Band Extension of Pseudo Relative Velocity Spectra of Strong Motion”, Department of Civil Engineering Report CE 94-02, University of Southern California, Los Angeles, CA.

Trifunac, MD and Todorovska, MI 1996. “Nonlinear soil response—1994 Northridge, California earthquake”, *Journal of Geotechnical Engineering*, ASCE, Vol. 122, No. 9, pp. 725–737.

Trifunac, MD and Todorovska, MI 1997a. “Response spectra and differential motion of columns”, *Earthquake Engineering and Structural Dynamics*, Vol. 26, No. 2, pp. 251–268.

Trifunac, MD and Todorovska, MI 1997b. “Northridge, California, earthquake of 1994: Density of red-tagged buildings versus peak horizontal velocity and intensity of shaking”, *Soil Dynamics and Earthquake Engineering*, Vol. 16, No. 3 pp. 209–222.

Trifunac, MD and Todorovska, MI 1997c. “Northridge, California, earthquake of 1994: Density of pipe breaks and surface strains”, *Soil Dynamics and Earthquake Engineering*, Vol. 16, No. 3, pp. 193–207.

Trifunac, MD, Ivanović, SS and Todorovska, MI 2001a. “Apparent periods of a building, I: Fourier analysis”, *Journal of Structural Engineering ASCE*, Vol. 127, No. 5, pp. 517–526.

Trifunac, MD, Ivanović, SS and Todorovska, MI 2001b. “Apparent periods of a building, II: Time-frequency analysis”, *Journal of Structural Engineering ASCE*, Vol. 127, No. 5, pp. 527–537.

Trifunac, MD, Ivanović, SS, Todorovska, MI, Novikova, EI, and Gladkov, AA 1999. “Experimental evidence for flexibility of a building foundation supported by concrete friction piles”, *Soil Dynamics and Earthquake Engineering*, Vol. 18, No. 3, pp. 169–187.

Trifunac, MD, Todorovska, MI and Ivanović, SS 1996. "Peak velocities and peak surface strains during Northridge, California, earthquake of 17 January 1994", *Soil Dynamics and Earthquake Engineering*, Vol. 15, No. 5, pp. 301–310.

Trifunac, MD, Todorovska, MI and Lee, VW 1998. "The Rinaldi strong motion accelerogram of the Northridge, California, earthquake of 17 January 1994", *Earthquake Spectra*, Vol. 14, No. 1, pp. 225–239.

Trifunac, MD, and Udawadia, FE 1974. "Parkfield, California, earthquake of June 27, 1966: A three-dimensional moving dislocation", *Bulletin of Seismological Society of America*, Vol. 64, No. 3, pp. 511–533.

Zanardo, G and Hao, H 1993. "Seismic response of multi-span simply supported bridges to a spatially varying earthquake ground motion", *Earthquake Engineering and Structural Dynamics*, Vol. 31, pp. 1325–1345.

Zembaty, Z, and Krenk, S 1993. "Spatial seismic excitations and response spectra", *Journal of Engineering Mechanics Div., ASCE*, Vol. 119, No. 12, pp. 2449–2459.

Zembaty, Z, and Krenk, S 1994. "Response spectra of spatial seismic ground motion", *10th European Conference on Earthquake Engineering*, Vol. 2, Vienna, Austria, pp. 1271–1275.

Zerva, A 1991. "Effect of spatial variability and propagation of seismic ground motions on the response of multiply supported structures", *Probabilistic Engineering Mechanics*, Vol. 6, No. 3–4, pp. 212–221.

APPENDIX A

Shown in Figure A1a, is the model we consider in this paper. It is essentially the same model as the one studied by Jalali et al. (2012) with only difference being the location of the pins in the central span. Previously those pins were located above the columns, while in this paper they are at distances a and b from the left and right supports of the central span. Consequently the following formulation of the equilibrium equations is almost identical to the formulation presented in Appendix A of Jalali et al. (2012). Nevertheless, for completeness of this presentation, we include the corresponding equations for the model studied here, and again outline the method of solution. We define the parameters of the model as follows

k_ϕ = Initial bending stiffness of the piers

c_ϕ = Linear bending damping coefficient of the piers

k_{T_c} = Initial torsional stiffness of the piers

c_{T_c} = Linear torsional damping coefficient of the piers

m_i = Mass of i -th rigid deck

$m = m_1 + m_2 + m_3$ = Total mass of the bridge

$L_1 = L_2 = L_3 = L$ = Length of each span of the bridge

$a = b = L/5$ = distance between middle hinge and the nearest pier

J_i = Polar moment of inertia of i -th rigid deck

h = The height of bridge

ϕ_i = Rotational angle of i -th pier

v_{g_i}, θ_{g_i} = The free field out-of-plane and torsional motions of ground surface at the base of i -th pier ($i = 1, 2, 3, 4$)

V_{G_i}, θ_{G_i} = Absolute out-of-plane and torsional motions of the center of gravity of i -th rigid deck ($i = 1, 2, 3$)

F_a, F_b = Forces in shear keys at the middle hinges

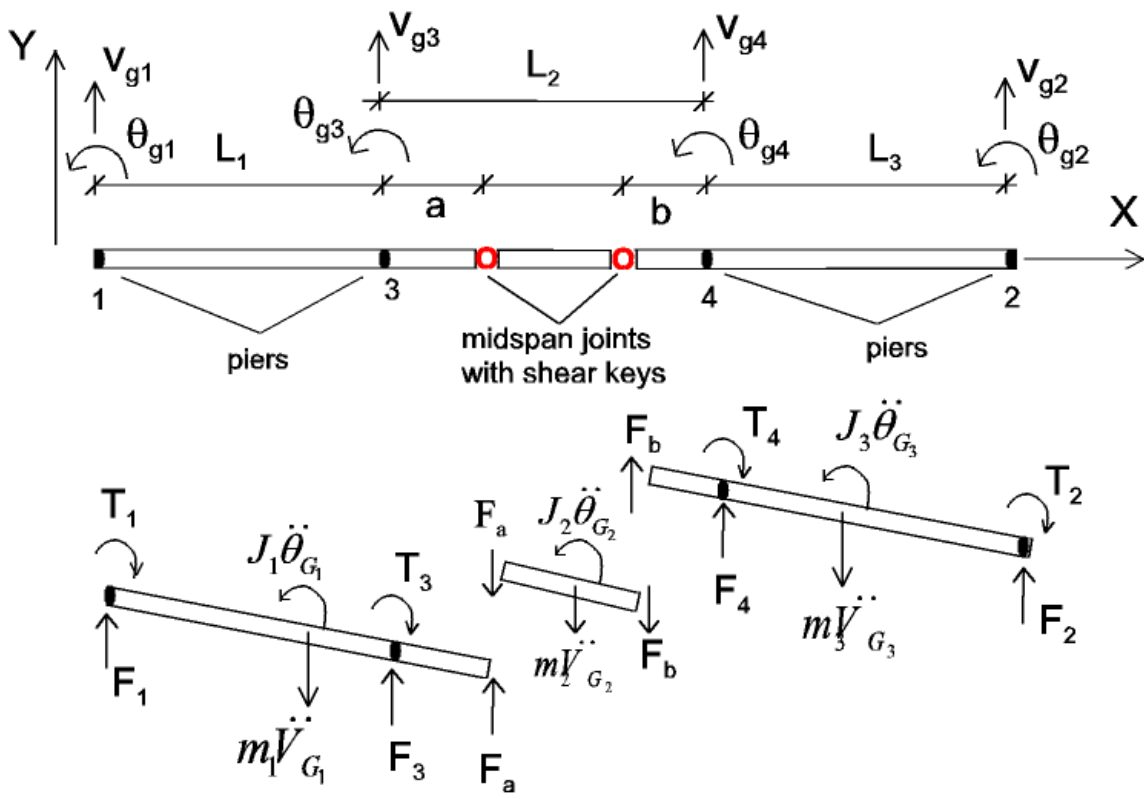


Fig. A1a. Plan view of the bridge

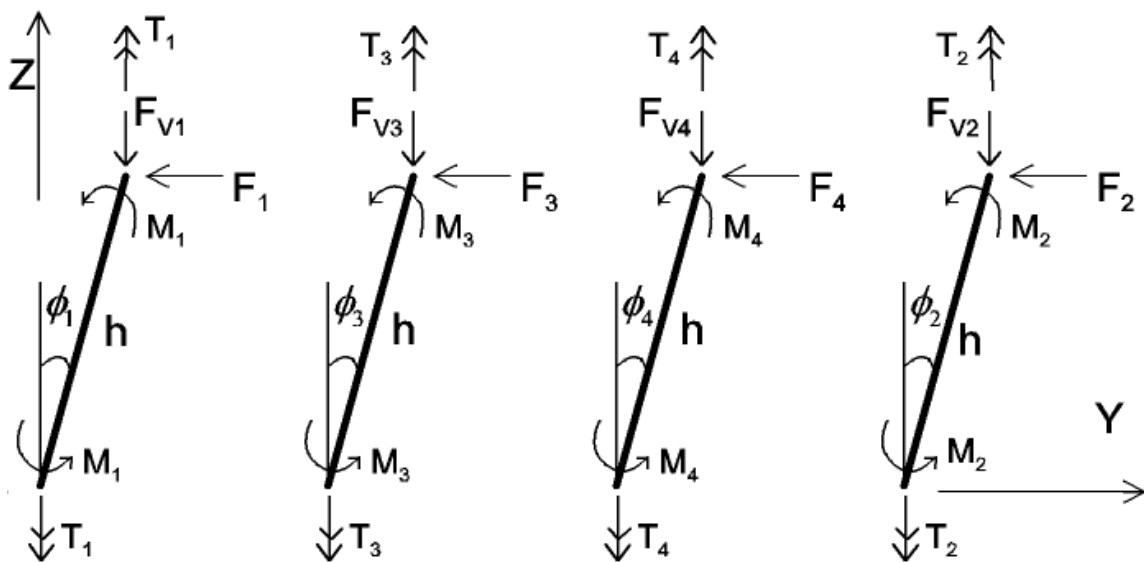


Fig. A1b. Side view of bridge piers and of the forces acting on them

From geometry of the model (Figures A1a,b) the absolute out-of-plane displacement and torsional rotation of the center of gravity of three rigid decks are

$$\begin{aligned}
V_{G_1} &= \frac{(L-a)}{2L}V_1 + \frac{(L+a)}{2L}V_3 = \frac{(L-a)}{2L}(V_{g_1} + h \sin \phi_1) + \frac{(L+a)}{2L}(V_{g_3} + h \sin \phi_3) \\
V_{G_3} &= \frac{(L-b)}{2L}V_2 + \frac{(L+b)}{2L}V_4 = \frac{(L-b)}{2L}(V_{g_2} + h \sin \phi_2) + \frac{(L+b)}{2L}(V_{g_4} + h \sin \phi_4) \\
V_a &= \frac{-a}{L}(V_{g_1} + h \sin \phi_1) + \frac{(L+a)}{L}(V_{g_3} + h \sin \phi_3) \\
V_b &= \frac{-b}{L}(V_{g_2} + h \sin \phi_2) + \frac{(L+b)}{L}(V_{g_4} + h \sin \phi_4) \\
V_{G_2} &= \frac{V_a + V_b}{2} = \frac{-a}{2L}(V_{g_1} + h \sin \phi_1) - \frac{b}{2L}(V_{g_2} + h \sin \phi_2) + \frac{(L+a)}{2L}(V_{g_3} + h \sin \phi_3) + \frac{(L+b)}{2L}(V_{g_4} + h \sin \phi_4) \\
\theta_{G_1} &= \sin^{-1}\left(\frac{V_1 - V_3}{L}\right) = \sin^{-1}\left\{\frac{1}{L}\left[(V_{g_1} - V_{g_3}) + h(\sin \phi_1 - \sin \phi_3)\right]\right\} \\
\theta_{G_2} &= \sin^{-1}\left\{\frac{\left[-a(V_{g_1} + h \sin \phi_1) + b(V_{g_2} + h \sin \phi_2) + (L+a)(V_{g_3} + h \sin \phi_3) - (L+b)(V_{g_4} + h \sin \phi_4)\right]}{L(L-(a+b))}\right\} \\
\theta_{G_3} &= \sin^{-1}\left(\frac{V_4 - V_2}{L}\right) = \sin^{-1}\left\{\frac{1}{L}\left[(V_{g_4} - V_{g_2}) + h(\sin \phi_4 - \sin \phi_2)\right]\right\}
\end{aligned} \tag{A1}$$

Differentiating with respect to time we obtain

$$\begin{aligned}
\dot{V}_{G_1} &= \frac{(L-a)}{2L}(\dot{V}_{g_1} + h \cos \phi_1 \dot{\phi}_1) + \frac{(L+a)}{2L}(\dot{V}_{g_3} + h \cos \phi_3 \dot{\phi}_3) \\
\ddot{V}_{G_1} &= \frac{(L-a)}{2L}(\ddot{V}_{g_1} - h \sin \phi_1 \dot{\phi}_1^2 + h \cos \phi_1 \ddot{\phi}_1) + \frac{(L+a)}{2L}(\ddot{V}_{g_3} - h \sin \phi_3 \dot{\phi}_3^2 + h \cos \phi_3 \ddot{\phi}_3) \\
\dot{\theta}_{G_1} &= \frac{\left[(\dot{V}_{g_1} - \dot{V}_{g_3}) + h(\cos \phi_1 \dot{\phi}_1 - \cos \phi_3 \dot{\phi}_3)\right]}{L \cos \theta_{G_1}} \\
\ddot{\theta}_{G_1} &= \frac{\left[(\ddot{V}_{g_1} - \ddot{V}_{g_3}) + h(\cos \phi_1 \ddot{\phi}_1 - \sin \phi_1 \dot{\phi}_1^2 - \cos \phi_3 \ddot{\phi}_3 + \sin \phi_3 \dot{\phi}_3^2)\right]}{L \cos \theta_{G_1}} + \tan \theta_{G_1} \dot{\theta}_{G_1}^2
\end{aligned}$$

$$\begin{aligned}
\dot{V}_{G_2} &= \frac{-a}{2L}(\dot{V}_{g_1} + h \cos \phi_1 \dot{\phi}_1) - \frac{b}{2L}(\dot{V}_{g_2} + h \cos \phi_2 \dot{\phi}_2) + \frac{(L+a)}{2L}(\dot{V}_{g_3} + h \cos \phi_3 \dot{\phi}_3) \\
&+ \frac{(L+b)}{2L}(\dot{V}_{g_4} + h \cos \phi_4 \dot{\phi}_4) \\
\ddot{V}_{G_2} &= \frac{-a}{2L}(\ddot{V}_{g_1} - h \sin \phi_1 \dot{\phi}_1^2 + h \cos \phi_1 \ddot{\phi}_1) - \frac{b}{2L}(\ddot{V}_{g_2} - h \sin \phi_2 \dot{\phi}_2^2 + h \cos \phi_2 \ddot{\phi}_2) \\
&+ \frac{(L+a)}{2L}(\ddot{V}_{g_3} - h \sin \phi_3 \dot{\phi}_3^2 + h \cos \phi_3 \ddot{\phi}_3) + \frac{(L+b)}{2L}(\ddot{V}_{g_4} - h \sin \phi_4 \dot{\phi}_4^2 + h \cos \phi_4 \ddot{\phi}_4) \\
\dot{\theta}_{G_2} &= \frac{1}{L(L-(a+b))\cos\theta_{G_2}} \left\{ -a(\dot{V}_{g_1} + h \cos \phi_1 \dot{\phi}_1) + b(\dot{V}_{g_2} + h \cos \phi_2 \dot{\phi}_2) + (L+a)(\dot{V}_{g_3} + h \cos \phi_3 \dot{\phi}_3) \right. \\
&\left. - (L+b)(\dot{V}_{g_4} + h \cos \phi_4 \dot{\phi}_4) \right\} \\
\ddot{\theta}_{G_2} &= \frac{1}{L(L-(a+b))\cos\theta_{G_2}} \left\{ -a(\ddot{V}_{g_1} + h \cos \phi_1 \ddot{\phi}_1 - h \sin \phi_1 \dot{\phi}_1^2) + b(\ddot{V}_{g_2} + h \cos \phi_2 \ddot{\phi}_2 - h \sin \phi_2 \dot{\phi}_2^2) \right. \\
&\left. + (L+a)(\ddot{V}_{g_3} + h \cos \phi_3 \ddot{\phi}_3 - h \sin \phi_3 \dot{\phi}_3^2) - (L+b)(\ddot{V}_{g_4} + h \cos \phi_4 \ddot{\phi}_4 - h \sin \phi_4 \dot{\phi}_4^2) \right\} + \tan \theta_{G_2} \dot{\theta}_{G_2}^2 \\
\dot{V}_{G_3} &= \frac{(L-b)}{2L}(\dot{V}_{g_2} + h \cos \phi_2 \dot{\phi}_2) + \frac{(L+b)}{2L}(\dot{V}_{g_4} + h \cos \phi_4 \dot{\phi}_4) \\
\ddot{V}_{G_3} &= \frac{(L-b)}{2L}(\ddot{V}_{g_2} - h \sin \phi_2 \dot{\phi}_2^2 + h \cos \phi_2 \ddot{\phi}_2) + \frac{(L+b)}{2L}(\ddot{V}_{g_4} - h \sin \phi_4 \dot{\phi}_4^2 + h \cos \phi_4 \ddot{\phi}_4) \\
\dot{\theta}_{G_3} &= \frac{[(\dot{V}_{g_4} - \dot{V}_{g_2}) + h(\cos \phi_4 \dot{\phi}_4 - \cos \phi_2 \dot{\phi}_2)]}{L \cos \theta_{G_3}} \\
\ddot{\theta}_{G_3} &= \frac{[(\ddot{V}_{g_4} - \ddot{V}_{g_2}) + h(\cos \phi_4 \ddot{\phi}_4 - \sin \phi_4 \dot{\phi}_4^2 - \cos \phi_2 \ddot{\phi}_2 + \sin \phi_2 \dot{\phi}_2^2)]}{L \cos \theta_{G_3}} + \tan \theta_{G_3} \dot{\theta}_{G_3}^2
\end{aligned} \tag{A2}$$

The equilibrium equations of the three rigid decks are

$$\sum F = 0 \Rightarrow \begin{cases} F_1 + F_3 + F_a - m_1 \ddot{V}_{G_1} = 0 & \text{(A3-1)} \\ F_a + F_b + m_2 \ddot{V}_{G_2} = 0 & \text{(A3-2)} \\ F_b + F_4 + F_2 - m_3 \ddot{V}_{G_3} = 0 & \text{(A3-3)} \end{cases}$$

$$\sum M_G = 0 \Rightarrow \begin{cases} T_1 + T_3 + F_1 \frac{(L+a)}{2} \cos \theta_{G_1} - J_1 \ddot{\theta}_{G_1} - F_3 \frac{(L-a)}{2} \cos \theta_{G_1} - F_a \frac{(L+a)}{2} \cos \theta_{G_1} = 0 & \text{(A3-4)} \\ (F_b - F_a) \left(\frac{L-(a+b)}{2} \right) \cos \theta_{G_2} - J_2 \ddot{\theta}_{G_2} = 0 & \text{(A3-5)} \\ T_2 + T_4 + F_b \frac{(L+b)}{2} \cos \theta_{G_3} + F_4 \frac{(L-b)}{2} \cos \theta_{G_3} - F_2 \frac{(L+b)}{2} \cos \theta_{G_3} - J_3 \ddot{\theta}_{G_3} = 0 & \text{(A3-6)} \end{cases}$$

Substituting Equations (A3-1) and (A3-3) into other equations we find the independent equations of motion of the system as follows

$$-F_1 - F_2 - F_3 - F_4 + m_1 \ddot{V}_{G_1} + m_2 \ddot{V}_{G_2} + m_3 \ddot{V}_{G_3} = 0 \quad (\text{A3-2a})$$

$$T_1 + T_3 + F_1(L+a) \cos \theta_{G_1} + F_3 a \cos \theta_{G_1} - m_1 \ddot{V}_{G_1} \frac{(L+a)}{2} \cos \theta_{G_1} - J_1 \ddot{\theta}_{G_1} = 0 \quad (\text{A3-4a})$$

$$(m_3 \ddot{V}_{G_3} + F_1 + F_3 - m_1 \ddot{V}_{G_1} - F_2 - F_4) \left(\frac{L-a-b}{2} \right) \cos \theta_{G_2} = 0 \quad (\text{A3-5a})$$

$$T_2 + T_4 - F_2(L+b) \cos \theta_{G_3} - F_4 b \cos \theta_{G_3} - m_3 \ddot{V}_{G_3} \frac{(L+b)}{2} \cos \theta_{G_3} - J_3 \ddot{\theta}_{G_3} = 0 \quad (\text{A3-6a})$$

The equilibrium equation of i-th pier is

$$\sum M = 0 \Rightarrow 2M_i + F_i h \cos \phi_i - F_{V_i} h \sin \phi_i = 0 \Rightarrow F_i = F_{V_i} \tan \phi_i - \frac{2M_i}{h \cos \phi_i} \quad (\text{A4})$$

Assuming uniform distribution of mass over the length of the bridge decks we approximately determine F_{V_i} as follows

$$F_{V_1} = \left[\frac{m_1}{2} - (m_1 + m_2) \frac{a}{2L} \right] g$$

$$F_{V_2} = \left[\frac{m_3}{2} - (m_2 + m_3) \frac{b}{2L} \right] g \quad (\text{A5})$$

$$F_{V_3} = (m_1 + m_2) \left(\frac{L+a}{2L} \right) g$$

$$F_{V_4} = (m_2 + m_3) \left(\frac{L+b}{2L} \right) g$$

The bending and torsional moments of piers are then defined as follows (Figures A1c, d)

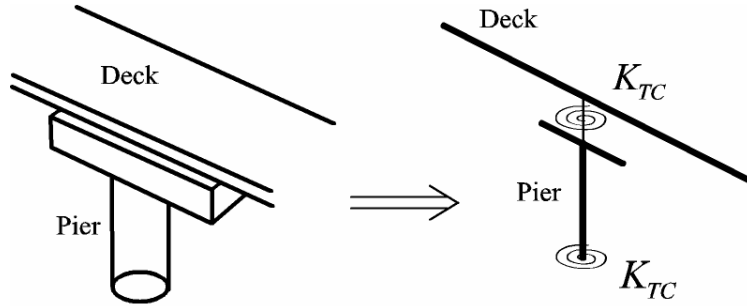


Fig. A1c. Schematic representations of torsional stiffness between the pier and the ground and between the pier and the deck

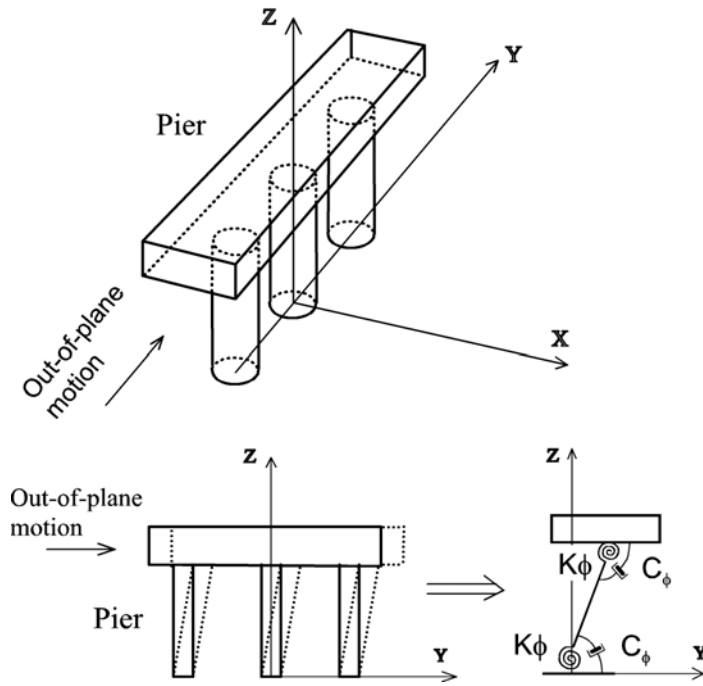


Fig. A1d. Schematic representation of the deformation of a pier and of the associated stiffness and damping

$$\begin{aligned}
 M_i &= K_\phi F(\phi_i) + C_\phi \dot{\phi}_i \\
 T_1 &= K_{T_c} \Phi(\theta_{g_1} - \theta_{G_1}) + C_{T_c} (\dot{\theta}_{g_1} - \dot{\theta}_{G_1}) \\
 T_2 &= K_{T_c} \Phi(\theta_{g_2} - \theta_{G_3}) + C_{T_c} (\dot{\theta}_{g_2} - \dot{\theta}_{G_3}) \\
 T_3 &= K_{T_c} \Phi(\theta_{g_3} - \theta_{G_1}) + C_{T_c} (\dot{\theta}_{g_3} - \dot{\theta}_{G_1}) \\
 T_4 &= K_{T_c} \Phi(\theta_{g_4} - \theta_{G_3}) + C_{T_c} (\dot{\theta}_{g_4} - \dot{\theta}_{G_3})
 \end{aligned} \tag{A6}$$

$F(\phi)$, and $\Phi(\phi)$ are nonlinear function of the type described in Fig. A2.

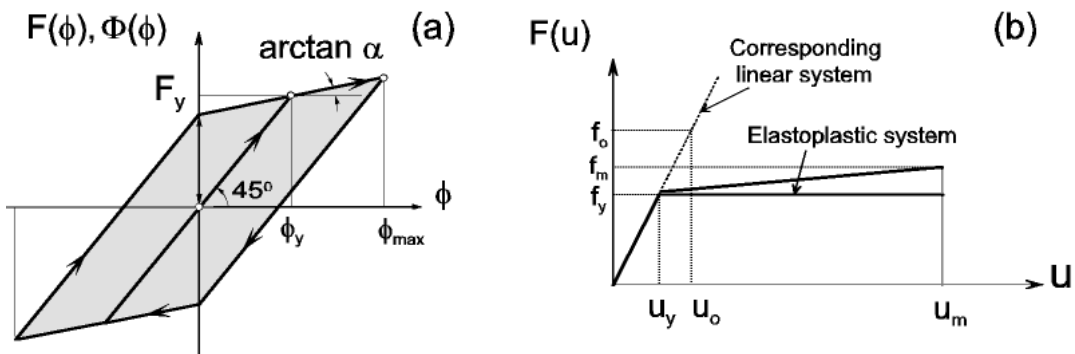


Fig. A2. Force-displacement (moment-rotation) relationship for bi-linear spring

From (A2), (A4), (A5), and (A6) one can write independent equations with respect to ϕ_1, ϕ_2, ϕ_3 , and ϕ_4 as follows

$$\begin{aligned}
& [-m_1(L-a) + m_2a] \frac{h \cos \phi_1}{2L} \ddot{\phi}_1 + [m_2b - m_3(L-b)] \frac{h \cos \phi_2}{2L} \ddot{\phi}_2 - (m_1 + m_2) \frac{(L+a)}{2L} h \cos \phi_3 \ddot{\phi}_3 \\
& - (m_2 + m_3) \frac{(L+b)}{2L} h \cos \phi_4 \ddot{\phi}_4 + \left[\frac{m_1}{2} - (m_1 + m_2) \frac{a}{2L} \right] g \tan \phi_1 - \frac{2M_1}{h \cos \phi_1} + \left[\frac{m_3}{2} - (m_2 + m_3) \frac{b}{2L} \right] g \tan \phi_2 \\
& - \frac{2M_2}{h \cos \phi_2} + (m_1 + m_2) \frac{(L+a)}{2L} g \tan \phi_3 - \frac{2M_3}{h \cos \phi_3} + (m_2 + m_3) \frac{(L+b)}{2L} g \tan \phi_4 - \frac{2M_4}{h \cos \phi_4} \\
& - \frac{m_1(L-a)}{2L} (\ddot{V}_{g_1} - h \sin \phi_1 \dot{\phi}_1^2) - \frac{m_1(L+a)}{2L} (\ddot{V}_{g_3} - h \sin \phi_3 \dot{\phi}_3^2) + \frac{m_2a}{2L} (\ddot{V}_{g_1} - h \sin \phi_1 \dot{\phi}_1^2) \\
& + \frac{m_2b}{2L} (\ddot{V}_{g_2} - h \sin \phi_2 \dot{\phi}_2^2) - \frac{m_2(L+a)}{2L} (\ddot{V}_{g_3} - h \sin \phi_3 \dot{\phi}_3^2) - \frac{m_2(L+b)}{2L} (\ddot{V}_{g_4} - h \sin \phi_4 \dot{\phi}_4^2) \\
& - \frac{m_3(L-b)}{2L} (\ddot{V}_{g_2} - h \sin \phi_2 \dot{\phi}_2^2) - \frac{m_3(L+b)}{2L} (\ddot{V}_{g_4} - h \sin \phi_4 \dot{\phi}_4^2) = 0
\end{aligned} \tag{A3-2b}$$

$$\begin{aligned}
& \left[\frac{-m_1(L^2 - a^2)}{4L} \cos \theta_{G_1} - \frac{J_1}{L \cos \theta_{G_1}} \right] h \cos \phi_1 \ddot{\phi}_1 + \left[\frac{-m_1(L+a)^2}{4L} \cos \theta_{G_1} + \frac{J_1}{L \cos \theta_{G_1}} \right] h \cos \phi_3 \ddot{\phi}_3 \\
& + K_{T_c} \Phi(\theta_{g_1} - \theta_{G_1}) + C_{T_c} (\dot{\theta}_{g_1} - \dot{\theta}_{G_1}) + K_{T_c} \Phi(\theta_{g_3} - \theta_{G_1}) + C_{T_c} (\dot{\theta}_{g_3} - \dot{\theta}_{G_1}) - \frac{2M_1}{h \cos \phi_1} (L+a) \cos \theta_{G_1} \\
& \left[\frac{m_1}{2} - (m_1 + m_2) \frac{a}{2L} \right] g(L+a) \cos \theta_{G_1} \tan \phi_1 + \left[(m_1 + m_2) \frac{(L+a)}{2L} g a \cos \theta_{G_1} \tan \phi_3 \right] \\
& - \frac{2M_3}{h \cos \phi_3} a \cos \theta_{G_1} - \frac{m_1(L^2 - a^2)}{4L} \cos \theta_{G_1} (\ddot{V}_{g_1} - h \sin \phi_1 \dot{\phi}_1^2) - \frac{m_1(L+a)^2}{4L} \cos \theta_{G_1} (\ddot{V}_{g_3} - h \sin \phi_3 \dot{\phi}_3^2) \\
& - \frac{J_1}{L \cos \theta_{G_1}} (\ddot{V}_{g_1} - \ddot{V}_{g_3} - h \sin \phi_1 \dot{\phi}_1^2 + h \sin \phi_3 \dot{\phi}_3^2) - J_1 \tan \theta_{G_1} \dot{\theta}_{G_1}^2 = 0
\end{aligned} \tag{A3-4b}$$

$$\begin{aligned}
& \left[\frac{-m_1(L-a)(L-(a+b))}{2L} \cos \theta_{G_2} + \frac{J_2 a}{L(L-a-b) \cos \theta_{G_2}} \right] h \cos \phi_1 \ddot{\phi}_1 + \left[\frac{m_3(L-b)(L-(a+b))}{2L} \cos \theta_{G_2} \right. \\
& \left. - \frac{J_2 b}{L(L-a-b) \cos \theta_{G_2}} \right] h \cos \phi_2 \ddot{\phi}_2 + \left[\frac{-m_1(L+a)(L-a-b)}{2L} \cos \theta_{G_2} - \frac{J_2(L+a)}{L(L-a-b) \cos \theta_{G_2}} \right] h \cos \phi_3 \ddot{\phi}_3 \\
& + \left[\frac{m_3(L+b)(L-a-b)}{2L} \cos \theta_{G_2} + \frac{J_2(L+a)}{L(L-a-b) \cos \theta_{G_2}} \right] h \cos \phi_4 \ddot{\phi}_4 + \frac{m_3(L-b)(L-a-b)}{4L} \cos \theta_{G_2} \\
& (\ddot{V}_{g_2} - h \sin \phi_2 \dot{\phi}_2^2) + \frac{m_3(L+b)(L-a-b)}{4L} \cos \theta_{G_2} (\ddot{V}_{g_4} - h \sin \phi_4 \dot{\phi}_4^2) + \left\{ \left[\frac{m_1}{2} - (m_1 + m_2) \frac{a}{2L} \right] g \tan \phi_1 \right. \\
& \left. - \frac{2M_1}{h \cos \phi_1} - \left[\frac{m_3}{2} - (m_2 + m_3) \frac{b}{2L} \right] g \tan \phi_2 + \frac{2M_2}{h \cos \phi_2} + \frac{(m_1 + m_2)(L+a)}{2L} g \tan \phi_3 - \frac{2M_3}{h \cos \phi_3} + \frac{2M_4}{h \cos \phi_4} \right. \\
& \left. - \frac{(m_2 + m_3)(L+b)}{2L} g \tan \phi_4 - \frac{m_1(L-a)}{2L} (\ddot{V}_{g_1} - h \sin \phi_1 \dot{\phi}_1^2) - \frac{m_1(L+a)}{2L} (\ddot{V}_{g_3} - h \sin \phi_3 \dot{\phi}_3^2) \right\} \\
& \frac{(L-a-b)}{2} \cos \theta_{G_2} - \frac{J_2}{L(L-a-b) \cos \theta_{G_2}} [-a(\ddot{V}_{g_1} - h \sin \phi_1 \dot{\phi}_1^2) + b(\ddot{V}_{g_2} - h \sin \phi_2 \dot{\phi}_2^2) \\
& + (L+a)(\ddot{V}_{g_3} - h \sin \phi_3 \dot{\phi}_3^2) - (L+b)(\ddot{V}_{g_4} - h \sin \phi_4 \dot{\phi}_4^2)] - J_2 \tan \theta_{G_2} \dot{\theta}_{G_2}^2 = 0
\end{aligned} \tag{A3-5b}$$

$$\begin{aligned}
& \left[\frac{m_3(L^2 - b^2)}{4L} \cos \theta_{G_3} + \frac{J_3}{L \cos \theta_{G_3}} \right] h \cos \phi_2 \ddot{\phi}_2 + \left[\frac{m_3(L+b)^2}{4L} \cos \theta_{G_3} - \frac{J_3}{L \cos \theta_{G_3}} \right] h \cos \phi_4 \ddot{\phi}_4 \\
& + K_{T_c} \Phi(\theta_{g_2} - \theta_{G_3}) + C_{T_c} (\dot{\theta}_{g_2} - \dot{\theta}_{G_3}) + K_{T_c} \Phi(\theta_{g_4} - \theta_{G_3}) + C_{T_c} (\dot{\theta}_{g_4} - \dot{\theta}_{G_3}) \\
& - \left[\left(\frac{m_3}{2} - (m_2 + m_3) \frac{b}{2L} \right) g \tan \phi_2 - \frac{2M_2}{h \cos \phi_2} \right] (L+b) \cos \theta_{G_3} - \left[(m_2 + m_3) \frac{(L+b)}{2L} g \tan \phi_4 \right. \\
& \left. - \frac{2M_4}{h \cos \phi_4} \right] b \cos \theta_{G_3} + \frac{m_3(L^2 - b^2)}{4L} \cos \theta_{G_3} (\ddot{V}_{g_2} - h \sin \phi_2 \dot{\phi}_2^2) + \frac{m_3(L+b)^2}{4L} \cos \theta_{G_3} (\ddot{V}_{g_4} - h \sin \phi_4 \dot{\phi}_4^2) \\
& - \frac{J_3}{L \cos \theta_{G_3}} [\ddot{V}_{g_4} - \ddot{V}_{g_2} + h(-\sin \phi_4 \dot{\phi}_4^2 + \sin \phi_2 \dot{\phi}_2^2)] - J_3 \tan \theta_{G_3} \dot{\theta}_{G_3}^2 = 0
\end{aligned} \tag{A3-6b}$$

By considering

$$m = m_1 + m_2 + m_3$$

$$\alpha_{m_i} = \frac{m_i}{m} \tag{A7}$$

The above equations can be written in matrix form as follows

$$\begin{bmatrix} c_{11} & c_{12} & c_{13} & c_{14} \\ c_{21} & c_{22} & c_{23} & c_{24} \\ c_{31} & c_{32} & c_{33} & c_{34} \\ c_{41} & c_{42} & c_{43} & c_{44} \end{bmatrix} \begin{Bmatrix} \ddot{\phi}_1 \\ \ddot{\phi}_2 \\ \ddot{\phi}_3 \\ \ddot{\phi}_4 \end{Bmatrix} + \begin{bmatrix} c_{15} \\ c_{25} \\ c_{35} \\ c_{45} \end{bmatrix} = \begin{Bmatrix} 0 \\ 0 \\ 0 \\ 0 \end{Bmatrix} \quad (\text{A8})$$

where,

$$\begin{aligned} c_{11} &= [\alpha_{m_1}(L-a) - \alpha_{m_2}a] \frac{h \cos \phi_1}{2L} \\ c_{12} &= [-\alpha_{m_2}b + \alpha_{m_3}(L-b)] \frac{h \cos \phi_2}{2L} \\ c_{13} &= (\alpha_{m_1} + \alpha_{m_2}) \left(\frac{L+a}{2L} \right) h \cos \phi_3 \\ c_{14} &= (\alpha_{m_2} + \alpha_{m_3}) \left(\frac{L+b}{2L} \right) h \cos \phi_4 \\ c_{15} &= \left(\frac{-\alpha_{m_1}}{2} + (\alpha_{m_1} + \alpha_{m_2}) \frac{a}{2L} \right) g \tan \phi_1 + \frac{2M_1}{mh \cos \phi_1} + \left[\frac{-\alpha_{m_3}}{2} + (\alpha_{m_2} + \alpha_{m_3}) \frac{b}{2L} \right] g \tan \phi_2 + \frac{2M_2}{mh \cos \phi_2} \\ &\quad - (\alpha_{m_1} + \alpha_{m_2}) \frac{(L+a)}{2L} g \tan \phi_3 + \frac{2M_3}{mh \cos \phi_3} - (\alpha_{m_2} + \alpha_{m_3}) \frac{(L+b)}{2L} g \tan \phi_4 + \frac{2M_4}{mh \cos \phi_4} + \frac{\alpha_{m_1}(L-a)}{2L} \\ &\quad (\ddot{V}_{g_1} - h \sin \phi_1 \dot{\phi}_1^2) + \frac{\alpha_{m_1}(L+a)}{2L} (\ddot{V}_{g_3} - h \sin \phi_3 \dot{\phi}_3^2) - \frac{\alpha_{m_2}a}{2L} (\ddot{V}_{g_1} - h \sin \phi_1 \dot{\phi}_1^2) - \frac{\alpha_{m_2}b}{2L} (\ddot{V}_{g_2} - h \sin \phi_2 \dot{\phi}_2^2) \\ &\quad + \frac{\alpha_{m_2}(L+a)}{2L} (\ddot{V}_{g_3} - h \sin \phi_3 \dot{\phi}_3^2) + \frac{\alpha_{m_2}(L+b)}{2L} (\ddot{V}_{g_4} - h \sin \phi_4 \dot{\phi}_4^2) + \frac{\alpha_{m_3}(L-b)}{2L} (\ddot{V}_{g_2} - h \sin \phi_2 \dot{\phi}_2^2) \\ &\quad + \frac{\alpha_{m_3}(L+b)}{2L} (\ddot{V}_{g_4} - h \sin \phi_4 \dot{\phi}_4^2) \\ c_{21} &= \left[\frac{-3(L-a)}{L(L+a)} \cos \theta_{G_1} - \frac{1}{L \cos \theta_{G_1}} \right] h \cos \phi_1 \\ c_{22} &= 0, c_{24} = 0 \\ c_{23} &= \left(\frac{-3}{L} \cos \theta_{G_1} + \frac{1}{L \cos \theta_{G_1}} \right) h \cos \phi_3 \\ c_{25} &= \frac{K_{Tc}}{J_1} \Phi(\theta_{g_1} - \theta_{G_1}) + \frac{C_{Tc}}{J_1} (\dot{\theta}_{g_1} - \dot{\theta}_{G_1}) + \frac{K_{Tc}}{J_1} \Phi(\theta_{g_3} - \theta_{G_1}) + \frac{C_{Tc}}{J_1} (\dot{\theta}_{g_3} - \dot{\theta}_{G_1}) + 6 \left[1 - \left(1 + \frac{\alpha_{m_2}}{\alpha_{m_1}} \right) \frac{a}{L} \right] \\ &\quad \frac{g \cos \theta_{G_1}}{(L+a)} \tan \phi_1 - \frac{2M_1}{J_1 h \cos \phi_1} (L+a) \cos \theta_{G_1} + 6 \left(1 + \frac{\alpha_{m_2}}{\alpha_{m_1}} \right) \frac{a}{L(L+a)} g \cos \theta_{G_1} \tan \phi_3 - \frac{2M_3}{J_1 h \cos \phi_3} a \cos \theta_{G_1} \\ &\quad - \frac{3(L-a)}{L(L+a)} \cos \theta_{G_1} (\ddot{V}_{g_1} - h \sin \phi_1 \dot{\phi}_1^2) - \frac{3}{L} \cos \theta_{G_1} (\ddot{V}_{g_3} - h \sin \phi_3 \dot{\phi}_3^2) - \frac{1}{L \cos \theta_{G_1}} (\ddot{V}_{g_1} - \ddot{V}_{g_3} - h \sin \phi_1 \dot{\phi}_1^2 \\ &\quad + h \sin \phi_3 \dot{\phi}_3^2) - \tan \theta_{G_1} \dot{\theta}_{G_1}^2 \end{aligned}$$

$$\begin{aligned}
c_{31} &= \left[\frac{-3\alpha_{m_1}}{\alpha_{m_2}} \frac{(L-a)}{L(L-a-b)} \cos \theta_{G_2} + \frac{a}{L(L-a-b) \cos \theta_{G_2}} \right] h \cos \phi_1 \\
c_{32} &= \left[\frac{3\alpha_{m_3}}{\alpha_{m_2}} \frac{(L-b)}{L(L-a-b)} \cos \theta_{G_2} - \frac{b}{L(L-a-b) \cos \theta_{G_2}} \right] h \cos \phi_2 \\
c_{33} &= \left[\frac{-3\alpha_{m_1}}{\alpha_{m_2}} \frac{(L+a)}{L(L-a-b)} \cos \theta_{G_2} - \frac{(L+a)}{L(L-a-b) \cos \theta_{G_2}} \right] h \cos \phi_3 \\
c_{34} &= \left[\frac{3\alpha_{m_3}}{\alpha_{m_2}} \frac{(L+b)}{L(L-a-b)} \cos \theta_{G_2} + \frac{(L+b)}{L(L-a-b) \cos \theta_{G_2}} \right] h \cos \phi_4 \\
c_{35} &= \frac{3\alpha_{m_3}}{\alpha_{m_2}} \frac{(L-b)}{L(L-a-b)} \cos \theta_{G_2} (\ddot{V}_{g_2} - h \sin \phi_2 \dot{\phi}_2^2) + \frac{3\alpha_{m_3}}{\alpha_{m_2}} \frac{(L+b)}{L(L-a-b)} \cos \theta_{G_2} (\ddot{V}_{g_4} - h \sin \phi_4 \dot{\phi}_4^2) \\
&+ \frac{3g}{(L-a-b)} \cos \theta_{G_2} \left\{ \left[\frac{\alpha_{m_1}}{\alpha_{m_2}} - \left(\frac{\alpha_{m_1}}{\alpha_{m_2}} + 1 \right) \frac{a}{L} \right] \tan \phi_1 - \left[\frac{\alpha_{m_3}}{\alpha_{m_2}} - \left(1 + \frac{\alpha_{m_3}}{\alpha_{m_2}} \right) \frac{b}{L} \right] \tan \phi_2 + \left(\frac{\alpha_{m_1}}{\alpha_{m_2}} + 1 \right) \left(\frac{L+a}{L} \right) \tan \phi_3 \right. \\
&- \left. \left(1 + \frac{\alpha_{m_3}}{\alpha_{m_2}} \right) \left(\frac{L+b}{L} \right) \tan \phi_4 \right\} + \frac{(L-a-b) \cos \theta_{G_2}}{J_2 h} \left(\frac{-M_1}{\cos \phi_1} + \frac{M_2}{\cos \phi_2} - \frac{M_3}{\cos \phi_3} + \frac{M_4}{\cos \phi_4} \right) \\
&- \frac{3\alpha_{m_1}}{\alpha_{m_2}} \frac{(L-a)}{L(L-a-b)} \cos \theta_{G_2} (\ddot{V}_{g_1} - h \sin \phi_1 \dot{\phi}_1^2) - \frac{3\alpha_{m_1}}{\alpha_{m_2}} \frac{(L+a)}{L(L-a-b)} \cos \theta_{G_2} (\ddot{V}_{g_3} - h \sin \phi_3 \dot{\phi}_3^2) \\
&- \frac{1}{L(L-a-b) \cos \theta_{G_2}} [-a(\ddot{V}_{g_1} - h \sin \phi_1 \dot{\phi}_1^2) + b(\ddot{V}_{g_2} - h \sin \phi_2 \dot{\phi}_2^2) + (L+a)(\ddot{V}_{g_3} - h \sin \phi_3 \dot{\phi}_3^2) \\
&- (L+b)(\ddot{V}_{g_4} - h \sin \phi_4 \dot{\phi}_4^2)] - \tan \theta_{G_2} \dot{\theta}_{G_2}^2 \\
c_{41} &= 0, c_{43} = 0 \\
c_{42} &= \left[\frac{3(L-b)}{L(L+b)} \cos \theta_{G_3} + \frac{1}{L \cos \theta_{G_3}} \right] h \cos \phi_2 \\
c_{44} &= \left[\frac{3}{L} \cos \theta_{G_3} - \frac{1}{L \cos \theta_{G_3}} \right] h \cos \phi_4 \\
c_{45} &= \frac{K_{T_c}}{J_3} \Phi(\theta_{g_2} - \theta_{G_3}) + \frac{C_{T_c}}{J_3} (\dot{\theta}_{g_2} - \dot{\theta}_{G_3}) + \frac{K_{T_c}}{J_3} \Phi(\theta_{g_4} - \theta_{G_3}) + \frac{C_{T_c}}{J_3} (\dot{\theta}_{g_4} - \dot{\theta}_{G_3}) - 6 \left[1 - \left(1 + \frac{\alpha_{m_2}}{\alpha_{m_3}} \right) \frac{b}{L} \right] \\
&\frac{g \cos \theta_{G_3}}{(L+b)} \tan \phi_2 + \frac{2M_2}{J_3 h \cos \phi_2} (L+b) \cos \theta_{G_3} - 6 \left(1 + \frac{\alpha_{m_2}}{\alpha_{m_3}} \right) \frac{b}{L(L+b)} g \cos \theta_{G_3} \tan \phi_4 + \frac{2M_4}{J_3 h \cos \phi_4} b \cos \theta_{G_3} \\
&+ \frac{3(L-b)}{L(L+b)} \cos \theta_{G_3} (\ddot{V}_{g_2} - h \sin \phi_2 \dot{\phi}_2^2) + \frac{3}{L} \cos \theta_{G_3} (\ddot{V}_{g_4} - h \sin \phi_4 \dot{\phi}_4^2) - \frac{1}{L \cos \theta_{G_3}} (\ddot{V}_{g_4} - \ddot{V}_{g_2} - h \sin \phi_4 \dot{\phi}_4^2 \\
&+ h \sin \phi_2 \dot{\phi}_2^2) - \tan \theta_{G_3} \dot{\theta}_{G_3}^2
\end{aligned} \tag{A9}$$

For small deformation of a linear system and by neglecting the gravity, damping, input ground motion, and high-order terms, Equations (A3-2b), (A3-4b), (A3-5b), and (A3-6b) can be written as follows

$$[-m_1(L-a) + m_2a] \frac{h}{2L} \ddot{\phi}_1 + [m_2b - m_3(L-b)] \frac{h}{2L} \ddot{\phi}_2 - (m_1 + m_2) \frac{(L+a)}{2L} h \ddot{\phi}_3 - (m_2 + m_3) \frac{(L+b)}{2L} h \ddot{\phi}_4 - \frac{2K_\phi}{h} (\phi_1 + \phi_2 + \phi_3 + \phi_4) = 0 \quad (\text{A3-2c})$$

$$\left[\frac{-m_1(L^2 - a^2)}{4L} - \frac{J_1}{L} \right] h \ddot{\phi}_1 + \left[\frac{-m_1(L+a)^2}{4L} + \frac{J_1}{L} \right] h \ddot{\phi}_3 - \frac{2K_{T_c} h}{L} (\phi_1 - \phi_3) - 2K_\phi \frac{(L+a)}{h} \phi_1 - 2K_\phi \frac{a}{h} \phi_3 = 0 \quad (\text{A3-4c})$$

$$\left[\frac{-m_1(L-a)(L-a-b)}{4L} + \frac{J_2 a}{L(L-a-b)} \right] h \ddot{\phi}_1 + \left[\frac{m_3(L-b)(L-a-b)}{4L} - \frac{J_2 b}{L(L-a-b)} \right] h \ddot{\phi}_2 + \left[\frac{-m_1(L+a)(L-a-b)}{4L} - \frac{J_2(L+a)}{L(L-a-b)} \right] h \ddot{\phi}_3 + \left[\frac{m_3(L+b)(L-a-b)}{4L} + \frac{J_2(L+b)}{L(L-a-b)} \right] h \ddot{\phi}_4 - \frac{K_\phi}{h} (L-a-b)(\phi_1 - \phi_2 + \phi_3 - \phi_4) = 0 \quad (\text{A3-5c})$$

$$\left[\frac{m_3(L^2 - b^2)}{4L} + \frac{J_3}{L} \right] h \ddot{\phi}_2 + \left[\frac{m_3(L+b)^2}{4L} - \frac{J_3}{L} \right] h \ddot{\phi}_4 - 2K_{T_c} \frac{h}{L} (\phi_4 - \phi_2) + \frac{2K_\phi}{h} (L+b)\phi_2 + \frac{2K_\phi}{h} b\phi_4 = 0 \quad (\text{A3-6c})$$

If we assume that

$$m_1 = m_3, a = b \quad ,$$

then by taking the Fourier transform of Equations (A3-2c), (A3-4c), (A3-5c), and (A3-6c) we have

$$\left\{ \left[\alpha_{m_1} (L-a) \frac{h}{2L} - \alpha_{m_2} \frac{ah}{2L} \right] \omega^2 - \frac{2K_\phi}{mh} \right\} (\phi_1 + \phi_2) + \left[(\alpha_{m_1} + \alpha_{m_2})(L+a) \frac{h}{2L} \omega^2 - \frac{2K_\phi}{mh} \right] (\phi_3 + \phi_4) = 0 \quad (\text{A3-2d})$$

$$\left\{ \frac{(4L^2 + 2La - 2a^2) \alpha_{m_1} h \omega^2}{9L^3} - \frac{8}{3} \left[\frac{K_{T_c} h}{mL^3} + \frac{K_\phi (L+a)}{mL^2 h} \right] \right\} \phi_1 + \left[\frac{2(L+a)^2 \alpha_{m_1} h \omega^2}{9L^3} + \frac{8}{3} \left(\frac{K_{T_c} h}{mL^3} - \frac{K_\phi a}{mL^2 h} \right) \right] \phi_3 = 0 \quad (\text{A3-4d})$$

$$\begin{aligned} & \left\{ \left[\frac{\alpha_{m_1}(L^2 - 3aL + 2a^2)}{3L^3} - \frac{\alpha_{m_2}(aL - 2a^2)}{9L^3} \right] h\omega^2 - \frac{4}{3} \frac{K_\phi(L - 2a)}{mL^2h} \right\} (\phi_1 - \phi_2) \\ & + \left[\frac{(3\alpha_{m_1} + \alpha_{m_2})(L^2 - aL - 2a^2)}{9L^3} h\omega^2 - \frac{4}{3} \frac{K_\phi(L - 2a)}{mL^2h} \right] (\phi_3 - \phi_4) = 0 \end{aligned} \quad (\text{A3-5d})$$

$$\begin{aligned} & \left[\frac{-(4L^2 + 2aL - 2a^2)}{9L^3} \alpha_{m_1} h\omega^2 + \frac{8}{3} \frac{K_{T_c} h}{mL^3} + \frac{8}{3} \frac{K_\phi(L + a)}{mL^2h} \right] \phi_2 - \left[\frac{2(L + a)^2}{9L^3} \alpha_{m_1} h\omega^2 \right. \\ & \left. + \frac{8}{3} \frac{K_{T_c} h}{mL^3} - \frac{8}{3} \frac{K_\phi a}{mL^2h} \right] \phi_4 = 0 \end{aligned} \quad (\text{A3-6d})$$

The above equations can be written in matrix form as follows

$$\begin{bmatrix} c_{11} & c_{12} & c_{13} & c_{14} \\ c_{21} & c_{22} & c_{23} & c_{24} \\ c_{31} & c_{32} & c_{33} & c_{34} \\ c_{41} & c_{42} & c_{43} & c_{44} \end{bmatrix} \begin{Bmatrix} \phi_1 \\ \phi_2 \\ \phi_3 \\ \phi_4 \end{Bmatrix} = \begin{Bmatrix} 0 \\ 0 \\ 0 \\ 0 \end{Bmatrix} \quad (\text{A10})$$

where,

$$\begin{aligned} c_{11} = c_{12} &= \left[\alpha_{m_1}(L - a) \frac{h}{2L} - \alpha_{m_2} \frac{ah}{2L} \right] \omega^2 - \frac{2K_\phi}{mh} \\ c_{13} = c_{14} &= (\alpha_{m_1} + \alpha_{m_2})(L + a) \frac{h}{2L} \omega^2 - \frac{2K_\phi}{mh} \\ c_{21} &= \frac{(4L^2 + 2La - 2a^2)\alpha_{m_1} h\omega^2}{9L^3} - \frac{8}{3} \left[\frac{K_{T_c} h}{mL^3} + \frac{K_\phi(L + a)}{mL^2h} \right] \\ c_{22} = c_{24} &= 0 \\ c_{23} &= \frac{2(L + a)^2 \alpha_{m_1} h\omega^2}{9L^3} + \frac{8}{3} \left(\frac{K_{T_c} h}{mL^3} - \frac{K_\phi a}{mL^2h} \right) \\ c_{31} = -c_{32} &= \left[\frac{\alpha_{m_1}(L^2 - 3aL + 2a^2)}{3L^3} - \frac{\alpha_{m_2}(aL - 2a^2)}{9L^3} \right] h\omega^2 - \frac{4}{3} \frac{K_\phi(L - 2a)}{mL^2h} \\ c_{33} = -c_{34} &= \frac{(3\alpha_{m_1} + \alpha_{m_2})(L^2 - aL - 2a^2)}{9L^3} h\omega^2 - \frac{4}{3} \frac{K_\phi(L - 2a)}{mL^2h} \\ c_{41} = c_{43} &= 0 \\ c_{42} &= -c_{21} \\ c_{44} &= -c_{23} \end{aligned} \quad (\text{A11})$$

For nonzero solution of Equation (A10) the determinant of the coefficients should be zero. Therefore we have

$$|C| = \begin{vmatrix} c_{11} & c_{12} & c_{13} & c_{14} \\ c_{21} & 0 & c_{23} & 0 \\ c_{31} & c_{32} & c_{33} & c_{34} \\ 0 & c_{42} & 0 & c_{44} \end{vmatrix} = 0 \Rightarrow (c_{23}c_{31} - c_{21}c_{33})(c_{13}c_{21} - c_{11}c_{23}) = 0 \quad (\text{A12})$$

If, for example, $a = b = L/5$ then by solving of Equation (A12) one can find the natural frequencies of the bridge as follows

$$|C| = \left(0.013654 \frac{h^2}{L^2} \omega^4 - 0.462217 \frac{K_{T_c} h^2}{mL^4} \omega^2 - 0.37689 \frac{K_\phi}{mL^2} \omega^2 + 4.2667 \frac{K_\phi K_{T_c}}{m^2 L^4} + 2.1336 \frac{K_\phi^2}{m^2 L^2 h^2} \right) \\ \left(-0.0512 \frac{h^2}{L} \omega^4 + \frac{4}{3} \frac{K_{T_c} h^2}{mL^3} \omega^2 + 1.2053 \frac{K_\phi}{mL} \omega^2 - \frac{32}{3} \frac{K_\phi K_{T_c}}{m^2 L^3} - 5.333 \frac{K_\phi^2}{m^2 L h^2} \right) = 0$$

$$K_{T_c} = 0 \Rightarrow \begin{cases} \omega_1^2 = 5.9066 \frac{K_\phi}{mh^2} , & \omega_2^2 = 7.95 \frac{K_\phi}{mh^2} \\ \omega_3^2 = 17.6344 \frac{K_\phi}{mh^2} , & \omega_4^2 = 19.653 \frac{K_\phi}{mh^2} \end{cases}$$

$$\begin{cases} K_{T_c} = 0.5 K_\phi \\ \frac{L}{h} = 5 \end{cases} \Rightarrow \begin{cases} \omega_1^2 = 6.0 \frac{K_\phi}{mh^2} , & \omega_2^2 = 8.0217 \frac{K_\phi}{mh^2} \\ \omega_3^2 = 18.065 \frac{K_\phi}{mh^2} , & \omega_4^2 = 20.259 \frac{K_\phi}{mh^2} \end{cases}$$

$$\begin{cases} K_{T_c} = K_\phi \\ \frac{L}{h} = 5 \end{cases} \Rightarrow \begin{cases} \omega_1^2 = 6.08 \frac{K_\phi}{mh^2} , & \omega_2^2 = 8.0854 \frac{K_\phi}{mh^2} \\ \omega_3^2 = 18.5 \frac{K_\phi}{mh^2} , & \omega_4^2 = 20.8723 \frac{K_\phi}{mh^2} \end{cases}$$

$$\begin{cases} K_{T_c} = 1.5 K_\phi \\ \frac{L}{h} = 5 \end{cases} \Rightarrow \begin{cases} \omega_1^2 = 6.16 \frac{K_\phi}{mh^2} , & \omega_2^2 = 8.1425 \frac{K_\phi}{mh^2} \\ \omega_3^2 = 18.95 \frac{K_\phi}{mh^2} , & \omega_4^2 = 21.4935 \frac{K_\phi}{mh^2} \end{cases}$$

(A13)

From Equation (A13) it is seen that the effect of torsional stiffness of piers on the natural frequencies of the bridge is small. By neglecting of torsional stiffness and damping of piers, $K_{T_c} = 0, C_{T_c} = 0$, one can determine the rotational damping coefficients of the system for prescribed fraction of critical damping. The mass, stiffness, and damping matrices of the bridge are

$$[M] = mh \begin{bmatrix} 0.11467 & 0.00133 & 0.032 & -0.008 \\ 0.00133 & 0.11467 & -0.008 & 0.032 \\ 0.032 & -0.008 & 0.288 & 0.048 \\ -0.008 & 0.032 & 0.048 & 0.288 \end{bmatrix}, [K] = \begin{bmatrix} \frac{2K_\phi}{h} & 0 & 0 & 0 \\ 0 & \frac{2K_\phi}{h} & 0 & 0 \\ 0 & 0 & \frac{2K_\phi}{h} & 0 \\ 0 & 0 & 0 & \frac{2K_\phi}{h} \end{bmatrix}, [C] = \begin{bmatrix} \frac{2C_\phi}{h} & 0 & 0 & 0 \\ 0 & \frac{2C_\phi}{h} & 0 & 0 \\ 0 & 0 & \frac{2C_\phi}{h} & 0 \\ 0 & 0 & 0 & \frac{2C_\phi}{h} \end{bmatrix} \quad (A14)$$

The natural frequencies and symmetric and asymmetric mode shapes of the system are then obtained as follows (Fig. A3)

$$|K - \omega^2 M| = 0 \Rightarrow \begin{cases} \omega_1^2 = \frac{5.9066K_\phi}{mh^2}, \omega_2^2 = \frac{7.954K_\phi}{mh^2} \\ \omega_3^2 = \frac{17.635K_\phi}{mh^2}, \omega_4^2 = \frac{19.65K_\phi}{mh^2} \end{cases}, [\Phi] = \begin{bmatrix} 1 & 1 & 1 & 1 \\ 1 & -1 & 1 & -1 \\ 9.271 & 3.448 & -0.1078 & -0.289 \\ 9.271 & -3.448 & -0.1078 & 0.289 \end{bmatrix} \quad (A15)$$

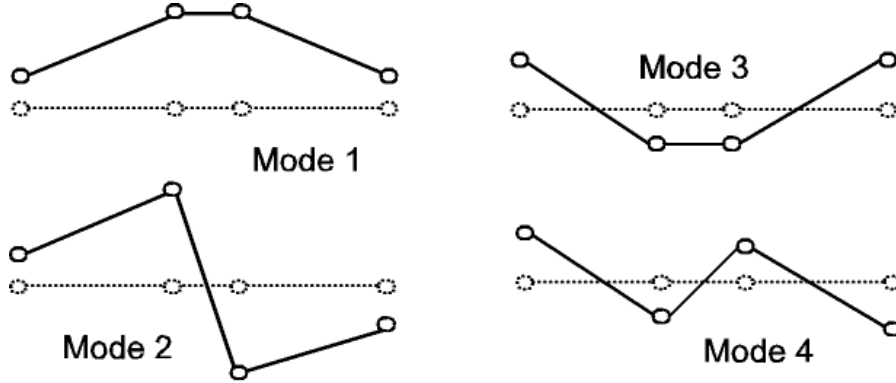


Fig. A3. Symmetric and antisymmetric mode shapes of the bridge

In modal space the mass, stiffness, and damping matrix of the bridge are

$$[M_n] = [\Phi]^T [M] [\Phi] = mh \begin{bmatrix} 58.9 & 0 & 0 & 0 \\ 0 & 6.485 & 0 & 0 \\ 0 & 0 & 0.2295 & 0 \\ 0 & 0 & 0 & 0.2206 \end{bmatrix}$$

$$\begin{aligned}
[K_n] &= [\Phi]^T [K] [\Phi] = \frac{K_\phi}{h} \begin{bmatrix} 347.81 & 0 & 0 & 0 \\ 0 & 51.56 & 0 & 0 \\ 0 & 0 & 4.05 & 0 \\ 0 & 0 & 0 & 4.334 \end{bmatrix} \\
[C_n] &= [\Phi]^T [C] [\Phi] = \frac{C_\phi}{h} \begin{bmatrix} 347.81 & 0 & 0 & 0 \\ 0 & 51.56 & 0 & 0 \\ 0 & 0 & 4.05 & 0 \\ 0 & 0 & 0 & 4.334 \end{bmatrix}
\end{aligned} \tag{A16}$$

The damping ratio of i -th mode is

$$\xi_i = \frac{C_i}{2M_i\omega_i} \tag{A17}$$

For the first mode we have

$$\xi_1 = 0.02 \Rightarrow \frac{C_\phi}{mh^2} = 0.00677\omega_1 \tag{A18}$$

APPENDIX B: NEAR-FAULT GROUND MOTION

It is difficult to predict strong ground motion near faults due to irregular distribution of slip (Mavroedis et al. 2004; Trifunac 1974; Trifunac and Udwadia 1974), non-uniform distribution of geologic rigidities surrounding the fault, irregular distribution of stress on the fault, and complex nonlinear processes that accompany fault motion during earthquakes. Thus, it is hard to predict the detailed nature of the near-fault ground motion and of the associated strong-motion pulses in time. In this study, a simplified approach is adopted, and these motions are modeled by smooth functions, which have correct average amplitudes and duration, and which have been calibrated against the observed fault slip and the recorded strong motions in terms of their peak amplitudes in time and their spectral content (Trifunac 1993a,b).

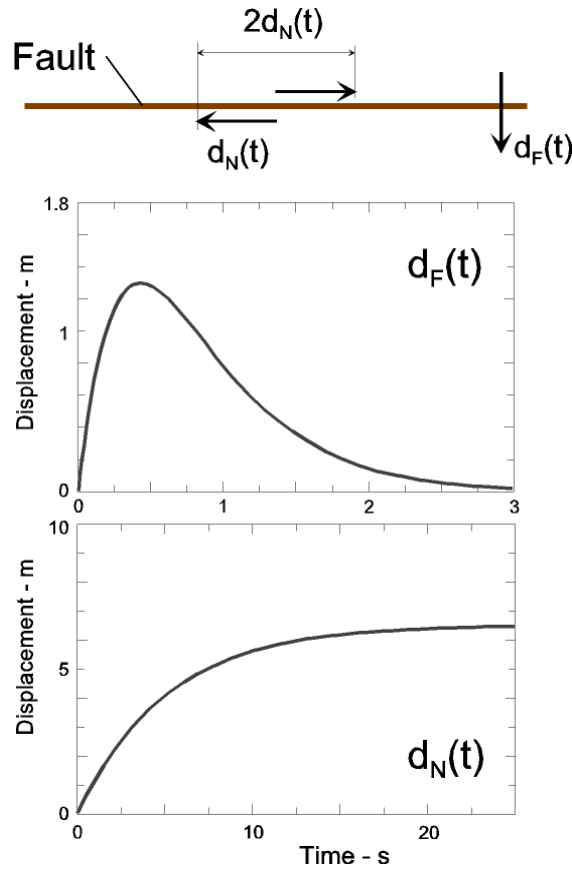


Fig. B1. Fault-parallel, $d_N(t)$, and fault-normal, $d_F(t)$, displacements for magnitude $M = 7$.

Figure B1 shows schematically a fault and two simple motions, d_N and d_F , which describe monotonic growth of the displacement toward the permanent static offset and a pulse, which is usually perpendicular to the fault surface and associated with failure of a nearby asperity or passage of dislocation under or past the observation point (Haskell 1969). In this paper the motions d_N and d_F represent fault-parallel and fault-normal motions of any fault system with shear type dislocation. For the fault-normal pulse, one can chose (Figure B1 -center)

$$d_F(t) = A_F t e^{-\alpha_F t}. \quad (\text{B1})$$

The values of A_F and α_F vs. earthquake magnitudes are shown in Table B1 (Trifunac 1993b). Because the strong-motion data are abundant only up to about $M = 6.5$, we place the values of α_F , A_F , τ_N , and A_N for $M = 7$ in Tables B1 and B2 in parentheses to emphasize that those are based on extrapolation. For the fault-parallel permanent displacement, one can consider (Figure B1 -bottom)

$$d_N(t) = \frac{A_N}{2} (1 - e^{-\frac{t}{\tau_N}}). \quad (\text{B2})$$

The values of A_N , and τ_N , vs. earthquake magnitudes are shown in Table B2 .

The amplitudes of d_F and d_N have been studied in numerous regression analyses of recorded peak displacements at various distances from the fault and in terms of the observed surface expressions of fault slip. The latter are traditionally presented as average dislocation amplitudes, \bar{u} , and are related to d_N , as $\bar{u} = 2d_N$ (see Figure B1 - top). An important property of d_F and d_N functions, as used in this study, is their initial velocity. It can be shown that $\dot{d}_F \sim \sigma\beta / \mu$, where σ is the effective stress (\sim stress drop) on the fault surface (Trifunac 1993b; Trifunac 1998), β is the velocity of shear waves in the fault zone, and μ is the rigidity of rocks surrounding the fault. For \dot{d}_N it can be shown that $\dot{d}_N = 0.5C_0\sigma\beta / \mu$, at $t = 0$, where typical values of C_0 are 0.6, 0.65, 1.00, 1.52, and 1.52 for $M = 4, 5, 6, 7$, and 8 (Trifunac 1993b; Trifunac 1998). The largest peak velocity observed so far, 5 to 10 km above the fault, is about 200 cm/s. For example, 170 cm/s was recorded during the Northridge, California earthquake of 1994 (Trifunac et al. 1998). Because there are no strong-motion measurements of peak ground velocity at the fault surface, the peak velocities \dot{d}_F and \dot{d}_N can be evaluated only indirectly in terms of σ . The accuracy of the stress estimates depends upon the assumptions and methods used in the interpretation of recorded strong-motion records, and it is typically about one order of magnitude. Therefore, by solving the above equations for σ , one can use $\sigma \sim 2\mu\dot{d}_N / (\beta C_0)$ and $\sigma \sim \mu\dot{d}_F / \beta$ to check their consistency with other published estimates of σ (Trifunac 2009).

Table. B1. Characteristics of Fault-Normal Pulse (Trifunac 1993b)

M (magnitude)	α_F (1/s)	A_F (cm/s)	$d_{F,\max}$ (cm)	$\dot{d}_{F,\max}$ (cm/s)
4	14.04	56.48	1.48	56.48
5	7.90	151.61	7.06	151.61
6	4.44	546.97	45.32	546.97
7	(2.50)	(860.34)	(126.6)	(860.34)

Table. B2. Characteristics of Fault-Parallel Displacement (Trifunac 1993b)

M (magnitude)	τ_N (s)	A_N (cm)	$d_{N,\max}$ (cm)	$\dot{d}_{N,\max}$ (cm/s)
4	0.55	4.9	2.45	4.45
5	1.2	29.2	14.6	12.17
6	1.8	245.5	122.75	68.19
7	(3.0)	(1288.0)	(644.0)	(214.7)